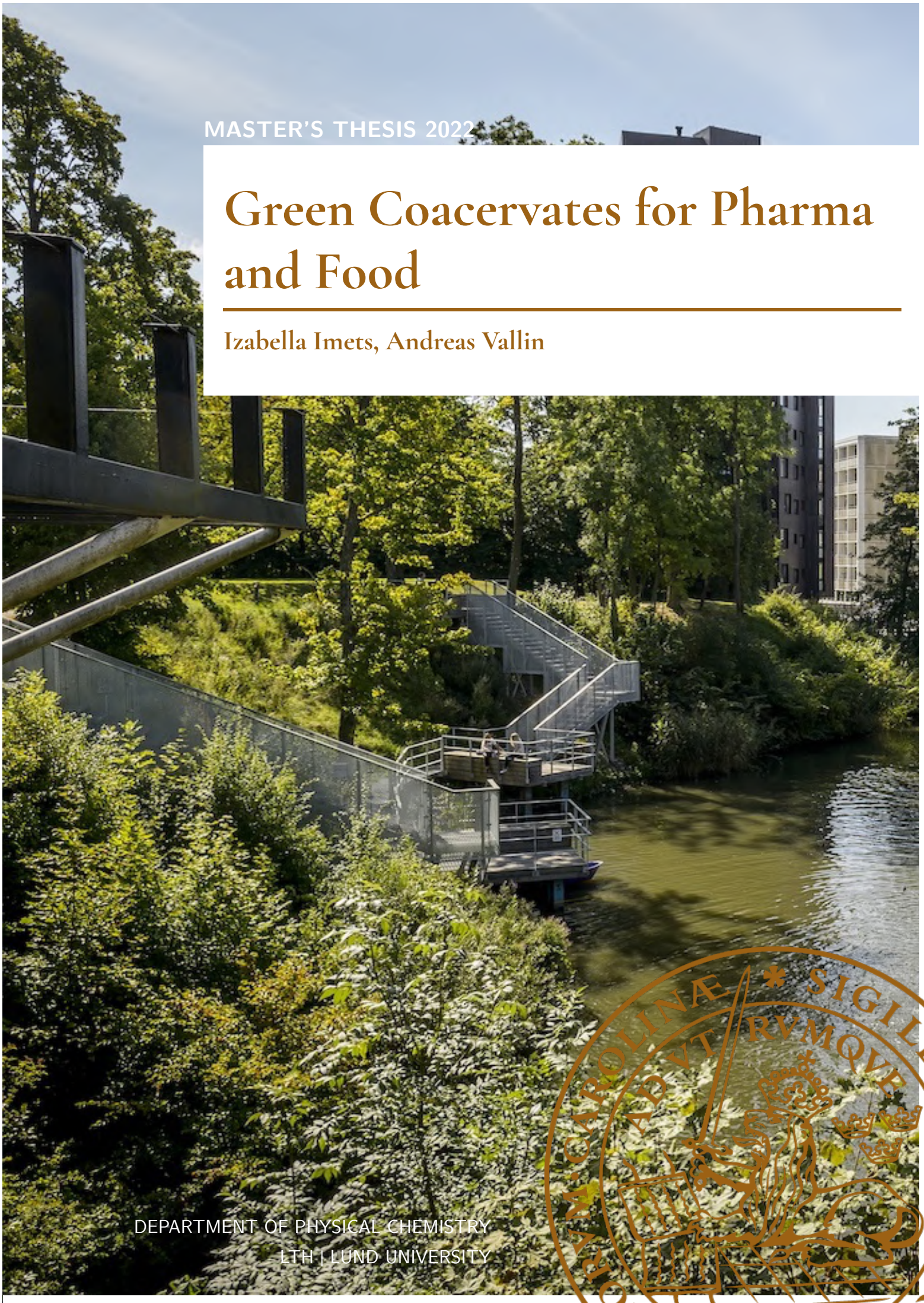

MASTER'S THESIS 2022

Green Coacervates for Pharma and Food

Izabella Imets, Andreas Vallin

DEPARTMENT OF PHYSICAL CHEMISTRY
LTH | LUND UNIVERSITY

MASTER THESIS
Physical Chemistry

Green Coacervates for Pharma and Food

Biobaserade surfaktant- och polymer system för läkemedel och livsmedel

Izabella Imets, Andreas Vallin

Green Coacervates for Pharma and Food

Izabella Imets
iz7884im-s@student.lu.se

Andreas Vallin
an1068va-s@student.lu.se

June 2022

Master's thesis work carried out at
the Department of Physical Chemistry, Lund University.

Supervisors: Marta Gubitosi, marta@crcom.com
Tommy Nylander, tommy.nylander@f1kem.lth.se

Examiner: Marie Wahlgren, marie.wahlgreen@food.lth.se

Abstract

Anionic biosurfactant-cationic biopolymer systems were investigated to identify and characterize a coacervation window. The characterization of the systems was performed with dynamic light scattering, small angle x-ray scattering and in-situ ellipsometry. The surfactants sodium- and potassium caprylate (NaC10, KC10) and sodium- and potassium laurate (NaC12, KC12) were studied with titration experiments, C10 had pKa 7.8 and C12 had pKa 8.6. The system needed to be above pH 9 for the surfactants to be soluble and form micelles. The studied biopolymers were QUATIN®- 350 TQ-D (Q350), 680 TQ-D (Q680) and N-Hance45 (N-Hance), in concentration range 0.5-2 wt%. The most studied system was NaC10-Q680 2 wt%. The coacervation area mapped out for this system was within the concentrations 1-2 wt% NaC10, which is around the critical micelle concentration (CMC). This was observed regardless of Q680 concentration. Therefore, the CMC was the main factor for coacervation since micelles are required for coacervation. Systems that exhibited coacervation could do this far from charge neutrality. Hence other factors play a role in coacervation.

Keywords: MSc; coacervate; biosurfactant; biopolymer;, SAXS; DLS; elliposometry.

Acknowledgements

We want to thank our supervisor, PhD. Marta Gubitosi at CR Competence for guiding us, helping shape this project, and always having time to discuss and answer questions. Thank you to PhD. Alessandra Del Giudice for guidance and understanding, especially with the SAXS analysis, where many workshops were needed. Thank you to Phd. Tobias Halthur for the help with interpreting and preforming the ellipsometry experiments, as well as always being available for an additional input. We would further like to thank both Tobias and PhD. Anna Stenstam at CR Competence for believing in and handing over the responsibility that this project has been. Further, we would like to thank our supervisor at LU, Prof. Tommy Nylander, for guidance and input. Additionally, thank you, PhD. Adrien Sthoer for helping with the ellipsometry. Thank you to Prof. Marie Wahlgren for being our examiner at LU and guiding us with the planing and feedback. Finally, we would like to thank everyone at CR Competence for a warm welcome to the team, always being available to help, and all the pleasant coffee breaks this last semester.

Division of work

This thesis was carried out by Andreas and Izabella equally when writing and forming the report. Izabella was more responsible for the laboratory part and sample preparation during the experimental phase. Meanwhile, Andreas did more data treatment and modelling for SAXS, DLS and ellipsometry. Overall, the work was divided equally.

Contents

Chapter 1
Introduction

This thesis is part of a Vinnova granted project in a collaboration between CR Competence AB and the group of Prof. Tommy Nylander at Physical Chemistry, Lund University. Moreover, the results of this thesis will lay the ground work for later studies within this project and contribute to knowledge to the coacervate field.

The need for more environmentally friendly, biodegradable and sustainable products is a great driving force for development today. The demand for products that are "free-from" specific ingredients are increasing due to legislation, consumer opinion and preferences towards more sustainable ingredients. Consequently, manufacturers desire to replace petroleum-based ingredients, like polymers and surfactants, with green and sustainable alternatives to satisfy this rising demand.

Furthermore, coacervates are an ingredient that is used for a number of different applications. Examples of usages are household cleaners and shampoos, but they are also used in food and pharmaceutical products for emulsification, texture purposes and drug delivery. A coacervate is a complex that is formed when two oppositely charged molecules in a aqueous solution interact with each other at specific concentration ratios, and liquid-liquid phase separation occurs. Commonly, coacervate systems consist of positively charged polymers and negatively charged surfactants.

The demands for greener products mentioned earlier also engulf products containing coacervates, promoting research and studies to replace fossil-based ingredients such as the surfactant sodium dodecyl sulfate with bio-alternatives in these systems. Although this research is in its early stages field, applications of these already exist today, for instance in shampoos and cosmetics.

Aim

The goal of this thesis is to contribute to the understanding of bio-ingredient-based coacervate systems and possibly find candidates to use in the development of commercial products. More specifically, the aim and goal of this thesis can split into the following steps.

- A set of biosurfactants and biopolymers has been chosen to be investigated individually and further evaluated for possible coacervate formation.
- If coacervation for the investigated system was found, these were further characterized. Partly to contribute to the understanding of coacervation and to understand this system for further studies.

Working with these bio-based systems gives rise to challenges, these are presented below.

Challenges

- These systems have not been studied thoroughly so far, therefore it cannot be stated for certain that the these greener systems will behave as the synthetic systems that are already known.
- Naturally derived materials usually are less refined, they might have a larger amount of impurities and lack very defined characteristics. For example, biopolymers in most cases have a broader distribution of molecular weight, contributing to more unpredictable behavior.

Procedure

Before studying the coacervate systems, the individual components must be assessed to see if they exhibit favourable properties. The main parameter to be evaluated here is the solubility, especially for the surfactant. The solubility of the surfactants was investigated with titration experiments. The individual components are also examined with SAXS and DLS to characterize these. Moreover, this data can help with interpreting the mixed systems. The surfactants and polymers evaluated in this project are presented in the table below.

Surafactants	Polymers
Capric acic (C10)	QUATIN® TQ-D 350
Lauric acid (C12)	QUATIN® TQ-D 680
	N-Hance™ CCG 45

After the evaluation of the single ingredients, it is necessary to understand which system(s), combinations of surfactant and polymer, are more promising to focus on. The characterization will be performed with DLS, SAXS, and ellipsometry. Secondly, by building a phase map of the system(s), it will be possible to assess if the system form coacervates within a relevant concentration range. This thesis will result in the characterization of these systems and understanding which parameters are essential to control coacervation. The thesis was carried out with monthly meetings to present and evaluate laboratory work results. At the meetings, the project's next step was discussed, and deadlines for the next time were decided.

Chapter 2
Background

2.1 Surfactans

Surfactants are substances with a specific structure consisting of two different functional groups with different affinities - a hydrophobic group and a hydrophilic group. Thanks to this specific structure, they can form self-assembled structures called micelles in solutions and absorb to the interface between two different phases, the solution and another phase (solid, gas, etc.). Surfactants are divided into ionic and non-ionic. The ionic surfactants are further branched into cationic, anionic or amphoteric surfactants, where the hydrophilic group of the surfactant dissociates into ions. Non-ionic surfactants does not dissociate into ions[1].

Surfactants are solubilized in water at low concentrations. However, when the concentration increases beyond a certain threshold, called critical micelle concentration (CMC), they spontaneously start self-assembling in solution into micelles. A way of determining CMC is by measuring the surface tension as a function of the surfactant concentration, which will give a similar curve to the Figure 2.1. As the surfactant concentration increases, the surfactants move to surfaces to minimize the system's free energy and decrease surface tension. When the CMC is reached, the surfactants self assemble into micellar structures, a favourable conformation, minimizing the surface free energy since the exposal of hydrophobic parts decreases. The surface tension remains relatively constant, or the decrease is smaller. Another phenomenon related to micelle formation, apart from the CMC, is called the critical aggregation concentration (CAC). Here surfactants can form pre micellar structures on solid surfaces or in surfactant-polymer mixtures [2].

To summarize, the formation of micelles is affected by three main forces: the repulsive hydrophobic forces between the hydrophobic tail and the solvent; electrostatic repulsion forces between hydrophilic heads after bonding of water, and increasing volume of the head (due to hydration of water); Van der Waals attractive forces between surfactant tails [3].

Furthermore, the physical behaviour of the surfactant is affected by ionic strength. By increasing the salinity content in a system the repulsion between hydrophilic head groups

decreases, hence facilitating the formation of micelles at a lower surfactant monomer concentration. The electrical charges at the surface of the micelles is also decreased by salt. Therefore, the CMC can be decreased with an increasing salt concentration in the system [3].

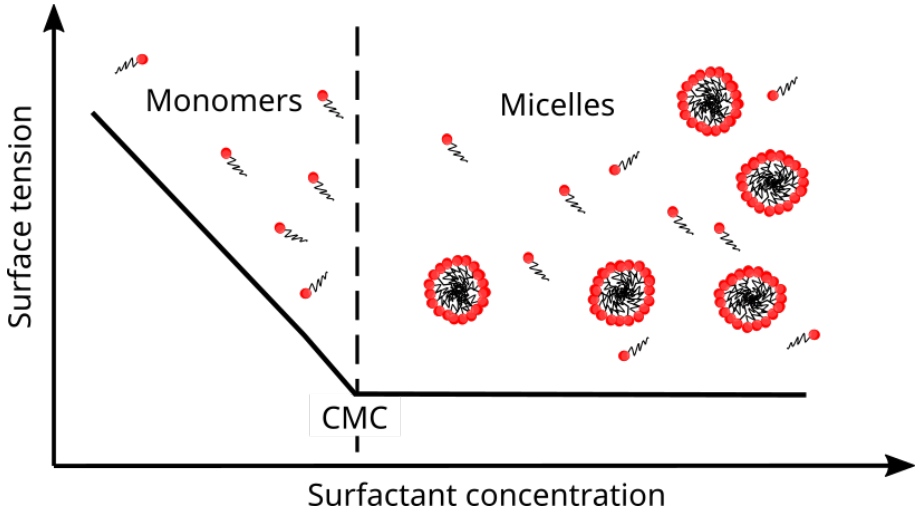

Figure 2.1: Illustration of a diagram with surface tension as a function of surfactant concentration. The critcal micelle concentration (CMC) is the change in the slope of the curve.

Moreover, the solubility of ionic surfactants in aqueous environments depends on the temperature and usually decreases at lower temperatures. The Krafft point is temperature specific for each surfactant, below which the surfactant's solubility decreases drastically. If the surfactant concentration is below the Krafft point but above the CMC, lamellae structure hydrated solid are formed [1].

2.1.1 Biosurfactants

The global market for surfactants was valued at 43.7 billion dollars in 2017, and in 2025 it is estimated to account for 66.4 billion dollars [4]. This accounts for 20 million tons of surfactants produced each year, and out of these, about 4% are biosurfactants. Biobased surfactants, or biosurfactants, are a growing market and span all markets in which conventional surfactants and detergents do: foods, pharmaceuticals, laundry detergents, cosmetics, personal care products, paints and coatings, to acknowledge a few [5]. The definition of biosurfactants is molecules that are entirely based on naturally derived biomass, such as sugars, plant oils, amino acids, etc. There are two different approaches to the production of biosurfactants; one is chemical, covalently linking hydrophobic and hydrophilic biobased molecules together; the other is biological, derived from plants or produced with biocatalysis(use of enzymes) or fermentation(microbes) [4]. There are four types of biobased surfactants: fatty acid-type, glycolipid-type, lipopeptide-type and polymer-type. The largest group of biobased surfactants are the fatty acid-type, which is the group focused on in this thesis [5].

Fatty acids may be difficult to dissolve in water due to their hydrophobic properties, i.e. the ionization state of the carboxyl group. It is thermodynamically more favourable for the carbon chain of the surfactant to leave the aqueous environment and be located inside

a micelle [6]. Moreover, as the chain length of the surfactant increases, the solubility in the aqueous environment decreases [7]. When a fatty acid reacts with a metal oxide or hydroxide, where the carboxylic acid is neutralized, a fatty acid soap is formed. Depending on the hydrocarbon chain melting temperature T_c in excess water and pH, it forms different physical states [7], see Figure 2.2. For example, to form micelles, the system needs to be above T_c for the fatty acid (1:1 acid-soap or soap) and equal to or above pH 9. Through equilibrium titration curves, the solubility can be examined [8].

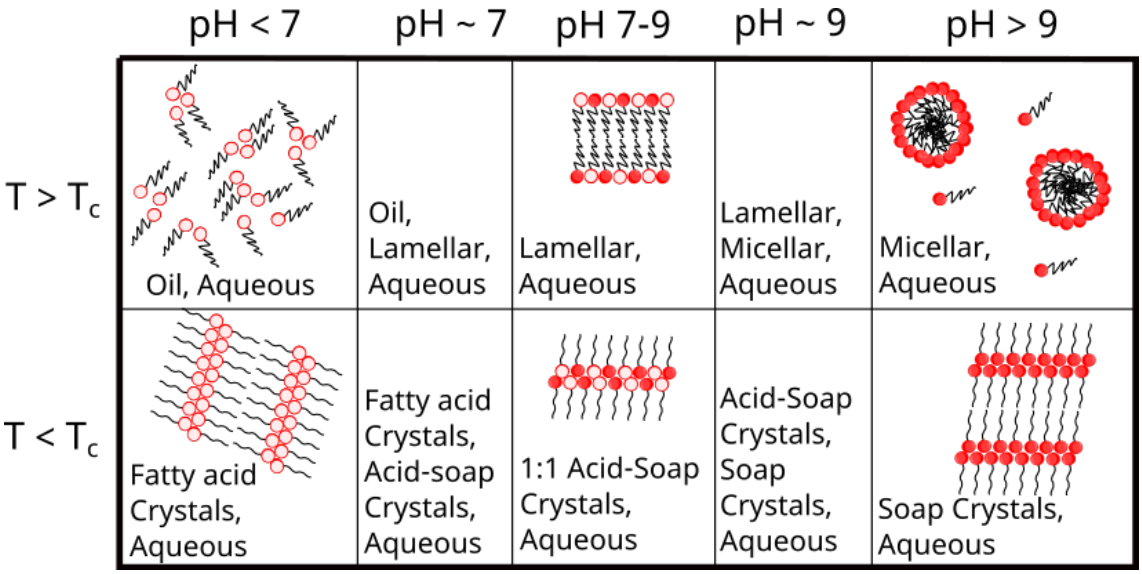

Figure 2.2: The physical behaviour of medium-chain($C \geq 10$) fatty acids and long-chain fatty acids, as a function of pH and chain melting temperature T_c. The open circles represent protonated surfactants and the closed circles represent ionized, anionic, surfactants. The squiggly lines of the surfactants represents unordered- and straight lines represents ordered hydrocarbon chains. Inspired by reference [8].

Capric acid and Lauric acid

The two biobased surfactants in this thesis are capric- and lauric acid. Capric acid has IUPAC name decanoic acid, a medium-chain fatty acid(MCFA) with 10 carbons (C10). It is present in coconut fat and palm kernel for approximately 6%. It can also be found in milk fat [9]. When capric acids are formed into salts, they are called caprate.

Lauric acid, IUPAC name dodecanoic acid, is another MCFA with 12 carbons (C12). Similar to capric acid, it is found in coconut fat, and palm kernel for approximately 50% [9]. When lauric acids are formed into salts, they are called laurate.

2.2 Biopolymers

The definitions of bio-ingredients, -polymers, -and degradable are diffuse, and there is no consensus in the literature and general. Although the unclarity, there are certificates and de-

mands for a polymer to be defined as biodegradable. Biopolymers are divided into two distinct subdivisions: those originating from fossil fuels and are biodegradable and those based on bio ingredients. However, the latter does not have to be biodegradable to be considered a biopolymer.[10]

Furthermore, this thesis only studies polysaccharide derivatives that originate from nature and thus classifies them into the latter category. Polysaccharide derivatives are the most common source of bio-ingredient based biopolymers. The molecular weight of polysaccharides is generally in the range of $10^4 - 10^7$ g/mol [10]. The monomers in polysaccharide chains are connected with glycosidic bonds. However, the side chains of these molecules can vary drastically and can contain inorganic compounds such as phosphates and sulfurs. This diversity in the side-chain groups allows for many different applications due to the various physical and chemical properties that the polysaccharide may exhibit. [10]

Moreover, the chain side chain group can be charged and give the polymer ionic properties. These ionic polymers are referred to as polyelectrolytes. Bio-based polyelectrolytesfrom derived from biopolymers are an attractive candidate for replacing fossil-based ingredients in cosmetics, pharmaceuticals, and nutrition. More specifically, products in these fields often include coacervates, and the goal is to replace the current fossil-based polymers with these biodegradable alternatives. The traditional synthesis of polymers that fossil allows the manufacturer to tailor the polymers, and therefore the polymer properties are well defined. Meanwhile, this is a challenge for biopolymers.[10]

Biopolymers that are naturally derived from nature have much more undefined physical and chemical properties, and these also include higher concentrations of impurities than synthetic ones. Moreover, a biopolymer's behaviour can vary heavily between batches, making it difficult to predict its effects. Due to this heavy dependence on batch behaviour, many iterations and extensive studies need to be done on biopolymers to conclude their behaviours. This Master thesis will primarily focus on the study of Hydroxypropyl trimonium inulin, commercially available as QUATIN®, and Guar hydroxipropyltrimonium chloride, commercially available as N-Hance™.

QUATIN®

Hydroxypropyl trimonium inulin is a novel cationic biopolymer provided by "Cosun Beet Company - Biobased Experts", called QUATIN®. It comes in various forms depending on the degree of modification and the ones used in this work are QUATIN®350 TQ-D and 680 TQ-D. Inulin, the backbone, has been reported to be a rather short polysaccharide with a chain length of 2-60 monomers[11]. More information on the physical and chemical properties of QUATIN is presented in table 3.2. QUATIN®is a derivative from the polysaccharide Inulin harvested and processed mainly from the Chicory root see Figure 2.3. QUATIN®is inulin with an added cationic side chain group at some monomer sites. More specifically, the hydroxyl group on the backbone has been replaced with Hydroxypropyltrimonium, which gives the polymer its cationic charge. Quatin is provided as a concentrated water solution which has background salinity, which increases as the charge density

Figure 2.3: Chicory root, the root that inulin is derived from.

of the polymer increases. QUATIN®has versatility and can therefore be used in various applications. It can be used to modify surfaces and in industrial applications. It is commonly used in personal skin care and hair products since it gives a moisturising effect.[12]

N-Hance™

N-Hance™ CCG 45 (N-Hance) is a product from Ashland and is based on the molecule Guar hydroxypropyltrimonium (Cat-Guar). Cat-Guar comes in the form of yellow and white powder, and it is processed from guar beans that come from the guar plant. An image of guar beans is presented in Figure 2.4. Guar is proceeded by first milling the beans to obtain the natural gum. When the gum is obtained, it needs to be purified and filtered. After that, it is exposed to epoxides to generate the product. The average degree of polymerization for natural Guar is around 3300 units [13] The world's major suppliers of guar beans are India, Pakistan, the United States, Australia and Africa. Cat-Guar has many different applications, but most focus on skincare and hair products. More information about the properties of Guar derivatives N-hance used in this thesis is presented in table 3.3.

Figure 2.4: Guar beans, that Cat-guar is synthesised from.

2.3 Coacervates

According to Bungenberg de Jong and Kruyt in 1929, coacervates were described as dense liquid droplets of macromolecules [14]. When referring to complex coacervation, multiple soluble molecules, out of at least one is a macromolecule (such as a polymer), co assemble with another molecule. The interactions results in the formation of two phases: a polymer dense and a polymer dilute phase. The dense polymer phase is the coacervate, whereas the low polymer concentration phase is the supernatant, also called the equilibrium phase[14].

The combination of oppositely charged surfactants and polymers is an example of coacervate formation. This is an essential combination for the functions of products within personal care, such as pharmaceuticals, food and cosmetics. This is due to a variety of properties of the components, like viscosity and complex states, that are possible to alter. For shampoos, specifically, anionic surfactants and cationic polyelectrolytes have been used since the 1970's [15] [16].

2.3.1 Coacervate complexes

Coacervation is the process where coacervates form and is defined as the process of when a colloidal dispersion of two immiscible separate liquid phases in the same medium occurs. The two phases are split into a dense phase with a high concentration of the colloidal particles, called the coacervate, which is in equilibrium with the dilute phase, often called the equilibrium phase. The morphology of the coacervate phase can remain as a turbid suspension of droplets, or the droplets can coalesce into a liquid phase. Moreover, depending on the density of this liquid phase, it can either be on top or the bottom of the equilibrium phase. This can be described as micro, or macrophase separation see Figure 2.5.

(a) (b)

Figure 2.5: Figure series showing the liquid-liquid phase separation of the coacervate system. This sample was investigated during the thesis and exhibited at first a microphase separation that after a few days, transitioned into a macrophase separation. (a) Microphase separation. (b) Macrophase separation.

It has been reported that both macromolecules in the coacervate phase have a mobility and can move relatively freely in this viscous phase [17]. Coacervation can be defined either as simple or complex. This thesis will focus on the complex variant. The simple mechanism only requires one colloidal ingredient, and coacervation can be promoted with additives such as salts and alcohols or by increasing the temperature. The coacervation, in this case, occurs because it generates and increases inter-colloid interactions of the colloidal agent and the medium. Meanwhile, the complex mechanism heavily depends on the charge ratio between the anionic and cationic components in the system. Parameters that affect the coacervation are molecular structure, pH, mixing ratio, ionic strength and temperature [17].

Coacevates system with anionic surfactants and cationic polymers in aqueous solutions change in formation depending on their ratios. An important parameter for coacervation is the electric equivalent molar ratio (S/P), where S is the moles of surfactant ions and P moles of the charges of the polymers. The ratio can help describe the dissolved states of oppositely charged surfactants and polymers coexisting in a solution, as illustrated in Figure 2.6.

In the illustration in Figure 2.6, when (S/P) < 1 and the surfactant concentration is below CMC, the surfactants all bind to the polar groups of the polymer. This is a single continuous mixed phase, including a net positive charge from the polymers. In the situation where (S/P) = 1, it is driven by the charge neutralization where more surfactants bind into the polymer, resulting in precipitation of the complex due to them becoming insoluble. CMC is reached in this case, and micelles are formed. This area is called the complex precipitation (CP) region or the coacervation region. Two phases are obtained here in thermodynamic equilibrium. When increasing the surfactant concentration (S/P) > 1, micelles are further formed on the precipitated complexes, giving rise to redissolution. Furthermore, the complexes and free micelles coexist, and the system goes back to being one phase [15]. It has also been reported that coacervation can also be promoted by hydrophobic interactions. i.e. it can happen below and above the charge neutrality point. Finally, at the optimal mixing ratio for coacervation, the complexes that are formed are neutral, and if there is a great excess of one of the ionic components, the complexes are moderately charged.[18]

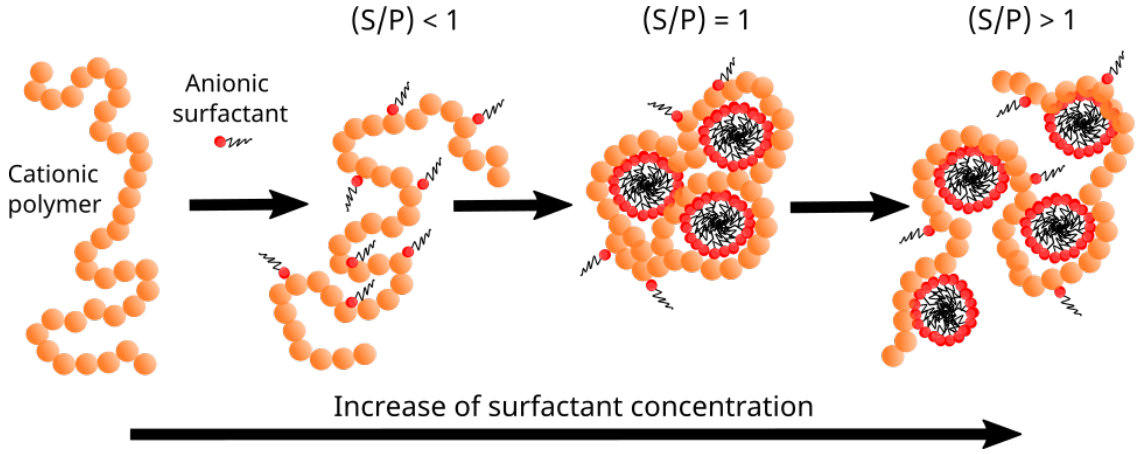

Figure 2.6: Illustration of the behaviour of surfactant and polymers in solution as a function of surfactant concentration, and charge ratio (S/P). Inspired by [15].

In the case of coacervation, the pH of the mixture determines the degree of ionization for the functional groups present. The coacervation mechanism is mostly driven by the reduction of free electrostatic energy, which decreases when two oppositely charged molecules in the system interact. So to have coacervation, it is crucial to be at a pH where both the macromolecules are in an ionized state. Otherwise, the coacervation will be inhibited or not happen to the same degree. Therefore, the optimal pH for coacervation depends on the pKa of the functional groups that generate the charge. Additionally, for some systems, the components' unionized version of the molecule is not soluble, and this is another property the pH governs, for instance, a fatty acid salt. The pH range for stable coacervation for any polymer system is narrow and heavily dependent on the system [18].

Ionic strength is another parameter that affects the coacervation process in the sample. The salt dissociates the coacervate complexes that form in the mixture. The presence of the salt weakens the electrostatic binding interactions between the macromolecules that form the coacervates. There is a term called the critical salt concentration, and if the system's salinity is above this, coacervation cannot occur. Additionally, different kinds of salt have various impacts on the systems. In some cases, the salt can promote coacervation where it otherwise does not happen. An example of this is when $CaCl_2$ was added to a system consisting of whey protein and Carrageenan, a linear sulfated polysaccharide. In this case, coacervation was possible above the protein's isoelectrical pH. The $CaCl_2$ was believed to act as a bridge between the negatively charged polymer and protein [19]. The same system is also reported to have increased coacervation when the concentration of NaCl was low, less than 45 mM. However, if the concentration of salt was increased to above 1 M, all coacervation was inhibited and is above the critical salt concentration [19].

The optimal mixing ratio between the two macromolecules that participate heavily depends on the studied system. More specifically, the optimal ratio is determined by the pH, salinity, nature of the macromolecules and the experimental set-up. However, the optimal pH for coacervation depends on the mixing ratios. Hence, there is a correlation between the parameters, making the systems difficult to understand fully. Molecular weight is also a factor that affects the coacervation of the system. Molecules with a high molecular weight tend to form gels or self-precipitates. On the other hand, molecules with a low molecular

weight instead ion pair with each other. The ion pairing of the molecules inhibits the coacervation process. Additionally, a very high concentration of the macromolecules can hinder their movements, making it difficult for them to undergo coacervation [18].

Chapter 3
Materials and Methods

3.1 Ingredients

In this thesis, the anionic biosurfactants and cationic biopolymers studied are seen in Table 3.1, 3.2 and 3.3, including supplier and properties.

Table 3.1: Surfactants, supplier and their properites.

Surfactant	Supplier	CAS	pKa
Capric acid (decanoic acid)	ThermoFisher	334-48-5	4.9
Lauric acid (dodecanoic acid)	ThermoFisher	143-07-7	5.3

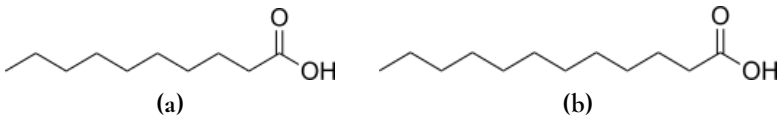

(a) (b)

Figure 3.1: Molecular structures of (a) Capric acid and (b) Lauric acid.

The surfactants are Capric acid (C10) and Lauric acid (C12), supplied as a white crystalline powder from Thermofisher. These surfactants were combined with sodium hydroxide (NaOH) or potassium hydroxide (KOH) to solubilize them into salts. These are sodium caprate (NaC10), potassium caprate (KC10), sodium laurate (NaC12) and potassium laurate (KC12). These salts have different CMC values: NaC10 has 86 mM/1.5 wt% with accepted values 80-110 mM and NaC12 has 30 mM/0.6 wt% with accepted values 7.15-30 mM [20]. The Krafft point of NaC10 is 38 ºC, and the Krafft point of the other salts is below room temperature.

There are three biopolymers investigated in this thesis. They consist of monomers modified with positively charged groups. Two of the biopolymers studied are hydroxypropyltrimonium inulin with the commercial name QUATIN®, CAS number 205131-94-8. Information about the properties can be found in Table 3.2 and the structure can be seen in Figure 3.2. They are non-toxic and biodegradable polymers with a high charge density according to the supplier [12]. The polymers have different degrees of substitution and overall molecular weights for the polymer chains, which results in different molecular weights per positive charge. These are specifically QUATIN® 350 TQ-D (Q350) and QUATIN® 680 TQ-D (Q680). The degree of substitution is higher for Q680, resulting in a higher charge density. According to the supplier Cosun, Q350 is supplied as a 41% and Q680 as a 40% active ingredient in water. The typical dosage levels for use in products are 0.5 to 2 wt%.

Table 3.2: The two inulin polymer types, supplier, NaCl content in product and properties.

Polymer	Supplier	NaCl (g/L)	Mw (g/L)	Degree of substitution	Mw per (+) charge
QUATIN® 350 TQ-D (Q350)	Cosun	68	~3000	0.35	587 g/mol
QUATIN® 680 TQ-D (Q680)	Cosun	105	~4000	0.68	368 g/mol

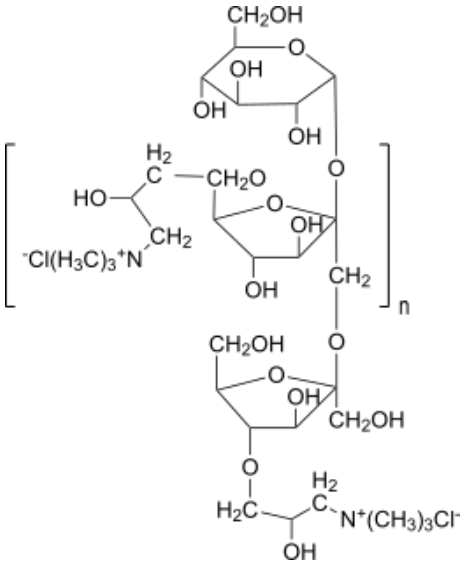

Figure 3.2: Molecular structure of QUATIN®.

The third biopolymer investigated is, Guar hydroxypropyltrimonium chloride, called N-Hance™ CCG 45 (N-Hance), CAS 65497-29-2 and 613-809-4, see Table 3.3. It is a cationic biopolymer with medium charge [21], with molecular structure seen in Figure 3.3. The polymer is supplied as a powder with pH 10.7 and viscosity 35 cps in a 1 wt% water mixture. Since this product has the lowest viscosity out of the N-Hance™-products that were candidates for this thesis, it is considered to have the lowest molecular weight per polymer chain out of them. The monomers is smaller for the QUATIN® polymer in comparison to the N-Hance; therefore, the N-Hance has a lower charge density. Recommendations for the use of N-Hance in formulations for shampoos and conditioners are 0.15-0.5 wt% and 0.4-1 wt% for liquid soaps and shower gels [21].

Table 3.3: Properties and other information of the polymer Guar Hydroxypropyltrimonium Chloride.

Polymer	Supplier	Viscosity (cps) for 1%	Mw per (+) charge
N-Hance™ CCG 45 (N-Hance)	Ashland	35	920 g/mol

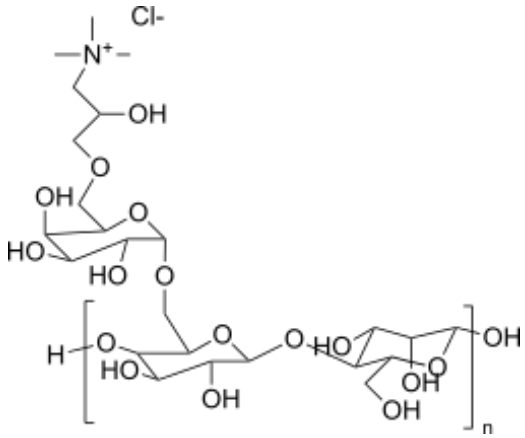

Figure 3.3: Molecular structure of N-Hance.

An important parameter is salinity. It influences the ionic strength of the self-assembly and aggregation behaviour of surfactants and polymers. The most common salt used today and present in nature is NaCl. It is additionally present as background salt in the polymer, as seen in Table 3.2. The highest percentage would be 0.525 wt% of NaCl for the samples with 2 wt% Q680. Consequently, a stock solution of 100 g/L NaCl was prepared, and the needed amount was added to each mixture to provide all samples with the same salinity content.

C10 and C12 are weak acids, soluble when deprotonated in their salt form. Therefore, pH is also an important parameter to keep into account. To stabilize and keep the pH constant, Tris buffer, tris(hydroxymethyl)aminomethane, $HOCH_2)_3CNH_2$, containing Trizma base and HCl, was used. A 200 mM Tris-stock solution was prepared with Trizma base and distilled water with addition from a 1 M HCl solution until reaching pH 9.

3.2 Single ingredient investigation

3.2.1 Surfactants

Titration experiments were performed to determine the solubility of the surfactants as a function of pH. The strong bases KOH and NaOH were used. Solutions of 10 wt% of surfactant were prepared. This was executed by weighing the corresponding amount of C10 respectively C12 into a vial, followed by the addition of distilled water. A 2 wt% surfactant solution in water was prepared on a later try with the same procedure. Known aliquots of the base were pipetted into the water-surfactant system and kept in agitation using a magnetic stirrer. A titration curve was obtained with pH as a function of the molar ratio between the hydroxide and moles surfactant. The C10 titrations were carried out in 22°C. The C12 was

more difficult to dissolve. Therefore, it was heated in a water bath with a water temperature of 40°C for 20 min before each addition of hydroxide. The pH measured was taken 5 min after the sample was removed from the heater. From these experiments, C10-salts were determined to be the surfactant continued with for the rest of the thesis, due to higher solubility and faster dissolution kinetics.

3.2.2 Polymers

According to the suppliers, the appropriate use for the polymers was approximately between 0.5-2 wt%. Therefore, polymer in water mixtures were prepared with these two percentages. The polymers were distributed as solutions (QUATIN®) or powder (N-Hance) and were put into distilled water directly. The salinity was adjusted with a 100 g/L NaCl-stock solution so that all samples had 0.525 NaCl wt%. In later stages of the investigation, 20 mM Tris was additionally added to each sample.

3.3 Bulk studies, sample preparation

3.3.1 Mixed systems

Dilution series were prepared with the mixtures summarized in the Table 3.4. They were prepared by mixing two mixtures for each dilution sample: with the **C10-salt 10 wt% solution** and either **polymer dilution** solution or **water dilution** solution. The dilution series followed the scheme: 10, 5, 2, 1, 0.5, 0.2 and 0.1 wt% C10-salt.

Table 3.4: Solutions with name and content summarized, used in the dilution series. '*' = Tris was included in the preparations of samples when buffer was intended, see "C10-salt 10 wt% V2".

Solution	Content
C10-stock solution	C10 (16-17 wt%) base, ratio (1:1) C10
C10-salt 10 wt% solution	C10-salt (10 wt%) polymer (0.5, 2 wt%) NaCl (0.525 wt%) Tris (20 mM)*
polymer dilution solution	polymer (0.5, 2 wt%) NaCl (0.525 wt%) Tris (20 mM)*
water dilution solution	NaCl (0.525 wt%) Tris (20 mM)*

Table 3.5: All the combinations for the dilution series that included QUATIN® polymers. The combinations are between surfactant-salt and polymer percentages. X = 10, 5, 2, 1, 0.5, 0.2, 0.1 wt% C10-salt.

	Polymer 0.5 wt%	Polymer 2 wt%
NaC10	x	x
KC10	x	x

Most QUATIN®-surfactant combinations were clear and water-like. Meanwhile, some exhibited turbidity. It was observed that samples that presented turbidity right after preparation lost turbidity over time if left standing on the bench for a couple of days. This was due to phase separation, with mostly two liquid phases observed. Therefore, different procedures were utilized to redisperse the phases before DLS and SAXS measurements, these are the following.

1. Manual shaking - proven not to be standardizable.
2. Oscillating mixer - samples were placed on the mixer for 5 minutes. It was observed that the turbidity was not recovered fully.
3. Sonication for 10 seconds - this yielded the least bubbles and reassured turbidity for all turbid samples.

The N-Hance-surfactant mixtures were mostly turbid and viscous, where the sonication procedure was solely used.

C10-stock solution. The preparation was according to the following procedure. A 1 M base stock solution was prepared. In a vial, the corresponding amount of C10 was weighed in, followed by the addition of an aliquot of a 1 M base stock solution. It was added to reach a molar ratio of 1:1 for C10:base. It was stirred overnight to get a clear solution. The pH was then measured to confirm that the pH was around 9, which is not far from a 1:1 C10:base solution.

C10-salt 10 wt% mixture, Version 1. Stock solutions containing C10-stock solution and 100 g/L NaCl were prepared. All polymers were added directly to the samples. Additionally, distilled double filtered water was prepared with the help of a syringe and filter Millipore Millex GV Hydrophilic PVDF 0.22 μm. The preparation is preformed according to the following list.

1. Weight in vial with magnetic stir bar and calculated amount of C10-stock solution.
2. Add double filtered distilled water and let the vial stir.
3. Slowly add polymer with a pipette (if solution), or weigh up separately (if powder) and add. Do this during stirring. Weigh the sample.
4. Add NaCl-stock solution with a pippette, if necessary.

5. Let sample stir until homogeneous.

The dilution series samples were prepared by weighing up this C10-salt 10 wt% solution and adding polymer- or water dilution solution. After preparation, the samples were visually inspected and even manually shaken if still not homogeneous. A picture was taken directly after preparation and after manually shaking the samples. Finally, the pH was measured.

C10-salt 10 wt% mixture, Version 2. The protocol was updated after investigating sample properties in terms of turbidity where improvements where found by refining the method of shaking and the addition of a buffer. The same stock solutions and filtered water as for V1 were prepared, in addition to a 200 mM Tris solution. The preparation is preformed according to the following list.

1. Weigh in vial with magnetic stir bar, and calculated amount of C10-stock solution.
2. Add double filtered distilled water and let the vial stir.
3. Add Tris and let the vial stir.
4. Slowly add polymer with a pipette (if solution), or weigh up separately (if powder) and add. Do this during stirring. Weigh the sample.
5. Addition of NaCl-stock solution with a pippette, if necessary.
6. Let sample stir until homogeneous.

The dilution series was prepared by weighing up this C10-salt 10 wt% solution and the addition of polymer- or water dilution solution. After preparation, the samples were visually inspected. Pictures were taken directly after preparation and after shaking with an oscillating mixer or sonication for 10 seconds. The pH was measured afterwards. Additionally, the samples were allowed to rest for three days. Pictures were taken before and after shaking(oscillating mixer or sonication), and then the pH was measured.

3.4 Scattering techniques

Scattering techniques are common for analyzing systems on the nanoscale where they allow determination of the size and shape of the system's entities. In turn, these are key to understand the macroscopic properties that eventually determine the behaviour of a product. However, this characterization is not trivial due to complex structures, varying length scales, etc. The type of radiation used by different scattering techniques varies and can be X-rays, electrons, light and neutrons. When a beam of a specific wavelength travels through a sample, different structures in the sample cause part of the beam to deviate from its path, i.e. be scattered. By locating a detector at different scattering angles θ, the intensity $I(\theta)$ of the scattered radiation at this angle can be detected as a function of time and angle.

Instead of comparing the scattering angle between different techniques, which would be inconvenient, the scattering vector $\vec{q}$ is preferred. The unit of q is inverse unit length, and the absolute value is calculated according to the expression below, where λ is the wavelength.

$$q = \frac{4\pi}{\lambda_0} sin(\frac{\theta}{2})$$

Different types of radiation, i.e. light, x-ray or neutrons, are appropriate depending on the length scale of interest and what property is to be characterized. The scattering of the beam is associated with the contrast, i.e. the difference between the objects and the matrix they are embedded in. X-ray scattering is associated with differences in electron density and is appropriate for the length scales 0.1-300 nm. Light scattering is associated with dielectric properties and refractive index, suitable for length scales 10 nm - 10 μm. Multiple scattering techniques are used to complement and observe a broader structure length range and assess different information that may be favourable.

Scattering is measured in similar ways by different instruments. To describe how the basic components are functioning, a reference image is presented in Figure 3.4.

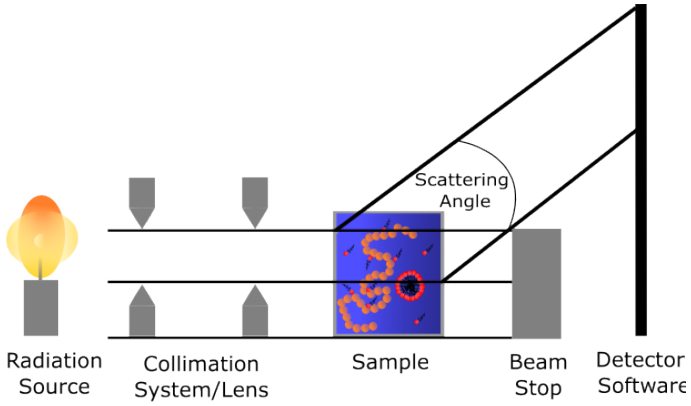

Figure 3.4: A schematic image of a scattering instrument and its basic components: beam source, collimation system/lens, sample, beam stop and detector software. Inspired by reference [22].

The radiation source, x-rays for SAXS and light for DLS, travels through a collimation system that narrows the beam and defines the zero-angle position. For SAXS, it is a system of slits and pinholes, and for DLS, it is lenses. As the beam irradiates the sample, it is subsequently scattered and ultimately detected by the detector as a function of angle. A beam stop is needed to block the transmitted source that has not been scattered. Otherwise, the transmitted radiation, which is very intense, would damage the detector and be the only signal detected. Since the scattered intensity is much lower than the transmitted and therefore be undetectable [22].

3.4.1 Dynamic Light Scattering

Dynamic Light Scattering (DLS) is used for obtaining the dynamic properties of a system, meaning the diffusion coefficient, size and size distribution. More specifically, the hydrodynamic radius (R_H), polydispersity (PDI) and particle size distribution (PSD) can be retrieved. It is used for turbidity measurements and for determining the average size of the complexes by obtaining the average hydrodynamic radius of particles. As the name states, it is a light scattering method, light as in a monochromatic, plane polarized light, belonging to the lights

in the visible spectrum. Fluctuation of the scattered intensity, caused by time-dependent fluctuations due to Brownian motion of the particles in solution, is detected at one certain angle at narrow time intervals (often ns-range). These scattered intensity fluctuations can be translated into the scattered intensity correlation function (ICF). The function compares the intensity $I(q,t)$ at a specific time t and the intensity I(q,t+τ) after a short delay time τ [23].

$$ICF = \frac{[I(q,t)I(q,t+\tau)]}{[I(q)]^2}$$

In this scenario, "correlation" is related to the memory of the particle's position. As the particle fluctuates from its initial position at time t, a memory of the initial condition is kept. As smaller particles diffuse faster, causing more fluctuating intensity, the memory decreases [23].

Measurements. DLS measurements were performed on a Zetasizer Nano ZS from Malvern Instruments Ltd, equipped with a He–Ne laser with a wavelength of 632.8 nm. The temperature of the measurement was set to 25 ºC, three measurements were performed for each sample, and the average was retrieved as data. There was no set measurement time. Instead, the machine optimised the measuring time for each sample. The samples were transferred and measured in disposable PMMA cuvettes of 1.5 ml with dimensions 12.5 × 12.5 × 45 mm and covered with a plastic lid.

Data interpretation. Although the DLS instrument is rather convenient to use, requiring short times and consistently providing value for PDI and R_H, the data retrieved from a DLS measurement is frequently far from trivial. For a meaningful measurement, it is crucial to understand what conditions need to be kept and how the intensity correlation function needs to be interpreted [23].

3.4.2 Small angle x-ray scattering

Small-angle x-ray scattering (SAXS) is used for investigating objects at the nanoscale. In particular, the following parameters can be retrieved: radius of gyration (R_G), the molecular weight (M_W), form factor ($P(q)$) and structure factor $S(q)$. In this analysis, the data treatment results in the scattered intensity $I(q)$-values in absolute scale, i.e. comparable from instrument to instrument, and background subtracted. Therefore, this technique is more extensive than DLS, mentioned above, both in preparation and in its analysis. SAXS is a small angle technique that focuses on angles close to 0º, specifically 0.1-10º. Since short wavelengths characterize x-rays, they are suitable for using shorter length scales, from Å to a couple of hundreds of nm, and larger q-ranges.

The inter- and intramolecular particle contributions to scattered intensity when measuring a monodisperse system in SAXS, is expressed as

$$I(q) = n\Delta\rho^2 P(q)S(q)$$

where n is the particle number density, $\Delta\rho$ is the contributing difference between particles and solvent, $S(q)$ is the structure factor, and $P(q)$ is the form factor.

When analyzing a mixture or a highly polydispersed structure, which most systems are, the analysis tends to be way more complex. It does not usually allow for quantitative size

and/or shape information. However, qualitative information may be obtained by using trends such as variation in concentration or temperature over time [23].

Measurements. Measurements are performed in the in-house instrument at the Division of Physical Chemistry, Lund University (JJ X-Ray Ganesha, Genix-3D Cu-Kalpha X-ray source and a Pilatus detector). As mentioned earlier, the background needs to be subtracted. Therefore, for a sample, two measurements need to be made—one of the matrix material and one of the whole sample scattering. The first mentioned is subtracted from the latter to obtain the particles' scattering. Additionally, an empty capillary needed to be measured to subtract the background from the signal. In conclusion, the following references were measured in addition to the samples, see list below. These references were needed for the data processing.

- Empty quartz capillary
- Water
- Water with salinity NaCl 0.525 wt%
- Water with salinity NaCl 0.525 wt% and 20 mM Tris.

The exposure time is crucial for reducing noise since the standard deviation of the experimental intensity is equal to the square root of the intensity. Thus, for good quality data, a longer exposure time is vital. However, it is inconvenient in aspects of time and economy.

At first, the measurements were performed over the sample holder at the neck of the capillary, i.e. the broader part of the capillary, see figure 3.5. The thickness at the neck of the capillary varied drastically between capillaries and was not homogeneous. This inhomogeneity in size gave the measured SAXS data a feature at high q-values, which was an issue. Therefore, in later measurements, it was decided to measure on hole 3 in the holder, where the capillaries were homogenous in size. The scattering signal at the highest q-values was partially shadowed by the sample holder. The shadowed portion of the scattering pattern was removed by reducing the two-dimensional integration angles of the signal from 0-360°to 50-310° for the configuration corresponding to high q-values.

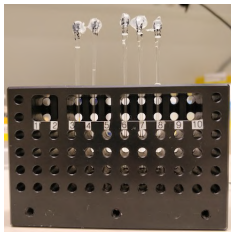

Figure 3.5: Samples filled in glass capillaries that has been sealed with glue on top. The samples are in capillary positions 3, 4 and 6-8 in the sample-holder.

The samples analyzed in this thesis are liquids, mainly consisting of water. All samples were measured in a disposable glass capillary with a thickness of ≈ 1.5 mm. First, the samples are filled with a syringe into the disposable glass capillaries. The capillaries are then sealed with a glue gun and then placed in a vertical sample holder and are then ready to be measured, as shown in Figure 3.5. The samples, 2 wt% NaC10-Q680 2 wt%, 1- and 2 wt% NaC10-N-Hance 2 wt%, were phase separated and therefore, it was of interest to measure the phases separately. The supernatant and gel phase of the sample were divided by extracting the supernatant carefully with a syringe into a different container. When extracting the respective phase with the syringe to transfer to the capillary, the syringe was below the system's surface to get a homogeneous, representative part of the phase.

Measurement settings. Two configurations were used one corresponding to low q (C23) and the other to high q (C21). The configurations have overlapping q ranges, and the corresponding measurement times are presented in table 3.6.

Table 3.6: Configurations used for the SAXS measurmenets, including q-value range and measurement times.

Configuration	q-value range [Å^{-1}]	Measurement time (s)
C21	0.1 < q < 2.75	900
C23	0.005 < q < 0.30	1800-2700

Data Treatment and Analysis. The collected two-dimensional scattering patterns were azimuthally averaged and normalized by transmission to obtain one-dimensional intensity vs. q profiles which were further processed with the software ATSAS [24], a commonly used software for data analysis of SAXS.

The data processing in ATSAS was done differently for the two configurations: C21 and C23, and the C21 had more steps in the processing. The data treatment for the C21 signal was performed in the following order. First, the length dependence of the intensity was removed by multiplying with the nominal thickness of the capillary. After this step, the empty capillary signal was subtracted from the signal, followed by the subtraction of the background signal from the sample. The background signal also had its capillary intensity and thickness dependence removed. Later, the signal was multiplied with the approximated thickness of the capillary to restore the thickness dependence. The intensity profile as a function of capillary thickness was used to determine this. Finally, the C23 intensity was scaled after the C21, and the data for the signals were concatenated at the q-value 0.185 Å^{-1} and for some N-hance samples at 0.1 Å Å^{-1}. All the same, steps were done for the C23 except that the empty capillary signal was not subtracted. The C23 signal corresponds to data from small q values where it is sensitive to these subtractions. The data range for q was then minimised to 0.012 to 1 Å as a final step. This q-range of the sample exhibits the feature this thesis addresses.

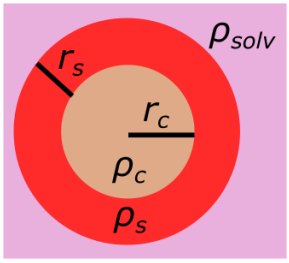

Figure 3.6: Visual representation of the core-shell model. The parameters are defined as r_c is the radius of the core, r_s is the radius from the core to the shell of the particle, ρ_c that is the scattering length density of the core, ρ_s scattering length density of the shell and ρ_{solv} is the scattering length density of the solvent.

The software SasView [25] was used for data plotting and modelling. The Debye function was used for approximating the parameters of the polymers [26]. Meanwhile, the core-shell model is applied for the surfactant [27]. The Debye function describes the scattering from the polymer chains subjected to the effects of excluded volume. Excluded volume is the volume of a single molecule in a system that is inaccessible to other molecules. In the Debye function, this is the volume of a single polymer chain. The model is used to describe the mass fractals of the polymer. The q-vector for the polymer model is expressed as the equation below. [25]

$$q = \sqrt{q_x^2 + q_y^2}$$

The equation for the polymer model applied to the data is presented in the equation below [?].

$$I(q) = I(0) \cdot \frac{2}{q^4 R_g^4}[exp(-q^2 R_g^2) - 1 + q^2 R_g^2] + bg \tag{3.1}$$

In the equation, R_g is the radius of gyration of the polymer chain, bg is the background intensity, and $I(0)$ is the intensity at $q = 0$. The core-shell sphere model is based on a spherical particle's form factor $P(q)$. In the model, the form factor is normalized by the particle volume. The form factor is expressed in the equation below.[27].

$$P(q) = \frac{scale}{V} F^2(q) + bg \tag{3.2}$$

Where $F(q)$ is defined in equation 3.3.

$$F(q) = \frac{3}{V_s}[V_c(\rho_c - \rho_s)\frac{sin(qr_c) - qr_c cos(qr_c)}{(qr_c)^3} + V_s(\rho_s - \rho_{solv})\frac{sin(qr_s) - qr_s cos(qr_s)}{(qr_s)^3}] \tag{3.3}$$

The parameters in equation 3.3 are defined as: V_s the volume of the whole spherical particle, V_c the volume of the core, r_c is the overall radius of the core, r_s is the radius from the core to the shell of the particle, ρ_c that is the scattering length density of the core, ρ_s scattering length density of the shell and ρ_{solv} is the scattering length density of the solvent. The charge densities and radii parameters are graphically presented in Figure 3.6.

3.5 In-situ ellipsometry

Ellipsometry is a widely used optical surface measurement technique to study the thickness and surface density of deposited materials on reflective surfaces. Moreover, the strength of the method and its usage in a plethora of different scientific fields is because it can analyze the optical properties with high accuracy for various materials such as organic films, oxides and adsorped organic complexes. In the coacervate field, ellipsometry is utilized to observe the deposition mechanism of the systems. One of the major purposes of coacervates in many products is to deposit on surfaces such as in shampoos. Therefore, ellipsometry is an excellent method to evaluate coacervation and product formulation with coacervates.

Ellipsometry is based on polarised light changes after reflecting on the sample surface from an incident beam. The ellipsometer measures the relative changes in amplitude (Ψ) and phase shift (Δ). Moreover, determining the thickness and reflective index of the deposited layer is done by parameters Ψ and Δ. In situ measurements can be done with ellipsometry. In-situ measurements for coacervate systems give insight into the adsorption mechanism for different coacervate formulations and how the mechanism is affected by changes in surfactant concentration, pH etc. The mechanism is studied by analyzing the changes in layer thickness and adsorbed amount. Furthermore, using Feijter's formula see equation 3.4, the adsorped amount per unit area for these systems is calculated. In the equation, the parameters have the following definition: n_0 is the refractive index of the bulk solution, n_f is the adsorbed layer's refractive index, and dn/dc is the refractive index increment of the adsorbed layer.[28]

$$\Gamma = d_f \frac{n_f - n_0}{dn/dc} \tag{3.4}$$

With the ellipsometer, the phase behaviour of the system, swelling, history dependence and dissolution experiments be studied for different parameters. One standard parameter to examine is the surfactant concentration. Furthermore, the ellipsometer reports the density of the adsorbed layer and how the packing density changes during the experiment. This gives insight into the most favourable configuration of the layer. Additionally, the systems' preference to deposit on hydrophobic or hydrophilic surfaces can be determined. Since ellipsometry allows the study of many different surfaces, usually silica is used, which can be processed to be either hydrophobic or hydrophilic.

3.5.1 Rinsing experiments, In-situ ellipsometry

The measurements were made on the automated Rudolph Research thin-film null ellipsometer, model 43603-200E, vertical alignment, and white light. The white light was filtered to be monochromatic with a wavelength of 402 nm. The method is based on measuring the changes in the state of polarization of light.

The deposition was studied on a hydrophilic silica wafer. The silica wafer was, before the experiments, stored in a base. After removing the wafer from the base, the wafer was cleaned with distilled water and dried with N_2-gun. Afterwards, it was sterilized in a plasma cleaner for five minutes.

Before the measurements could start, the refractive indexes n for the diluents: water-Tris-NaCl, Q680 2 wt% -Tris- NaCl and 10 wt% NaC10-Q680 2 wt% had to be determined. The data treatment needed these refractive indexes to determine the thickness and adsorped amount on the silica wafer. The refractometer was used to calculate the refractive indexes for the following three different wavelengths: 435 nm, 546 nm and 579 nm. Afterwards, the refractive index for the diluents at the wavelength 402 nm was obtained since the ellipsometer operates at this wavelength. These refractive indexes were extrapolated from equation 3.5, using the refractive index for the corresponding wavelengths determined in the refractometer earlier.

$$n = A + \frac{B}{\lambda^2} \tag{3.5}$$

Two rinsing experiments were done, one with the polymer dilution- and the other with the water dilution solvent. First, a 10 wt% NaC10-Q680 2 wt% mixture is transferred to the cuvette and measured. Then the rinsing experiment begins by starting the pumps that pump in the diluent with a 5 ml/min flow. A magnetic stirrer stirred the sample during the rinsing to ensure it was as homogeneous as possible. The same procedure was performed for both diluent agents. Afterwards, the data was processed and treated in Matlab.

Chapter 4

Results

4.1 Chapter one | Single ingredients

This chapter is about the individual characterization of the ingredients. Factors investigated were; solubility as a function of pH, visual appearance determined by viscosity, and turbidity.

4.1.1 Surfactants

Four titration experiments were performed to evaluate the solubility and pKa of 10 wt% C10 and C12 acid at room temperature. The fatty acids were titrated with NaOH and KOH. Moreover, the titration experiments as a function of the molar ratio of hydroxide and surfactant are presented in Figure 4.1.

There are different equilibria in the solutions. There is one equilibrium between the surfactant in its unprotonated acid form (solid) and ionized acid form (liquid), and one between the ionized acid form and acid-soap/salt form, see reaction below:

$$C_xOOH(s) \rightleftharpoons C_xOO^-(l) \rightleftharpoons C_xOO^-M^+(l)$$

where X is 10 or 12 and M is alkali metal, Na or K. The first equilibrium mentioned is a slow mechanism and needs to be considered in reaction kinetics. It can be increased through elevation of the temperature and stirring between measurements, which was a part of the protocol. Moreover, in the expression above, the equilibrium is driven to the right for each drop-wise addition of base to the solution, as more of the salt is formed. Therefore more of the surfactant is protonated and solubilized.

Furthermore, the C10-salts and KC12 are freely soluble, even below 0°C. However, NaC12 is insoluble below its Krafft point at 38°C [29]. For the C12 experiments, the samples were put in a water bath with a temperature of 40°C for 20 min between each data point. Moreover, the desired physical behaviour of the surfactant is micelles, which according to literature,

can only be formed at pH above 9 for medium-chain fatty acids 2.2. Therefore the studied systems in this thesis need to be above pH 9.

Data recorded before and after the addition of hydroxide to the samples can be seen in Figure 4.2. The surfactants were insoluble before any addition of base, and the samples were solubilized at an approximate equimolar addition of base, where most samples resulted in a water-like appearance. However, C12 acid titrated with NaOH had transitioned into a cream phase after a day of rest, see Figure 4.2. This is compatible with literature, where NaC12 is reported as insoluble below 38 °C[29].

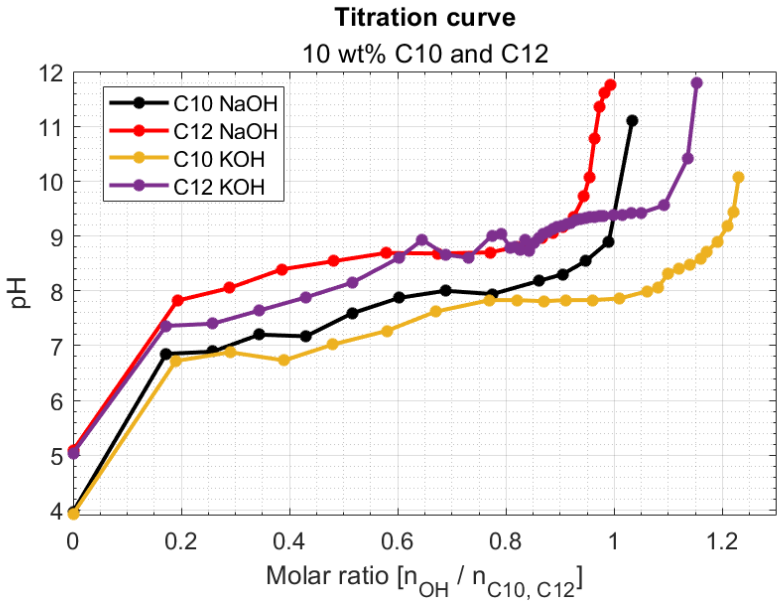

Figure 4.1: Titration curves of 10 wt% C10 and C12 acid titrated with bases NaOH and KOH.

As mentioned earlier, the reaction kinetics of C12 was slow and needed heating for the surfactant to solubilize at a reasonable time scale. Therefore it was rather complex to handle this larger fatty acid. Considering the challenges of working with C12, it was decided at this stage of the thesis that the investigation was to be continued with C10. These salts did not require heating to become soluble and therefore were more promising to focus on. Additional titration curves were made for the C10 surfactant. This time a lower concentration, 2 wt%, was used for more accurate measurements. A summarizing diagram for the titration curves of the different weight percentages is presented in Figure 4.3. The difference between the titration curves of different weight percentages is that the data points of the 2 wt% curves were more accurately mapping out the titration curve. Additionally, the 10 wt% titration curve titrated with KOH seems to deviate further away from its equivalence point compared to the other curves. Therefore the titration curve with 2 wt% C10 are more accurate. In conclusion, the pKa of the weak acid surfactants can be determined from these curves, which are equal to the point halfway to the equivalence point. For the C10, the pKa is approximately pH 7.6, and for C12, pKa is approximately 8.6.

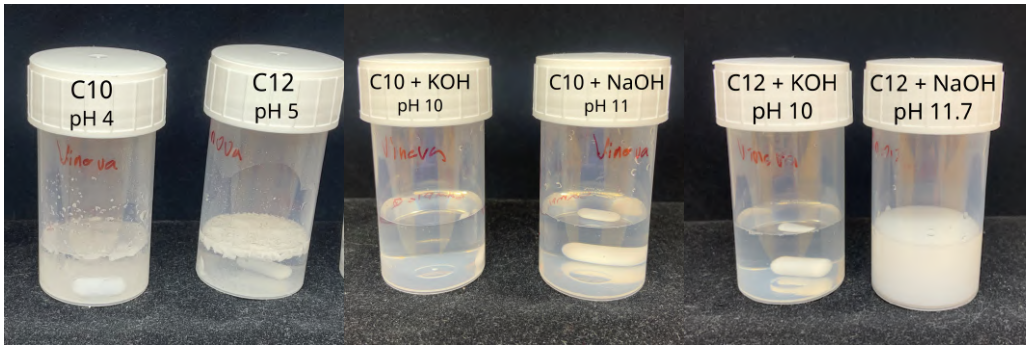

(a) (b) (c)

Figure 4.2: Visual appearance of 10 wt% C10 and C12 acids in water, before and after addition of base, including pH values. (a) Before addition of base, both C10 and C12 acids insoluble. (b) C10 samples after addition of base, solubilized. (c) C12 after addition of base, where KC12 sample became water-like and NaC12 sample exhibited cream-like texture.

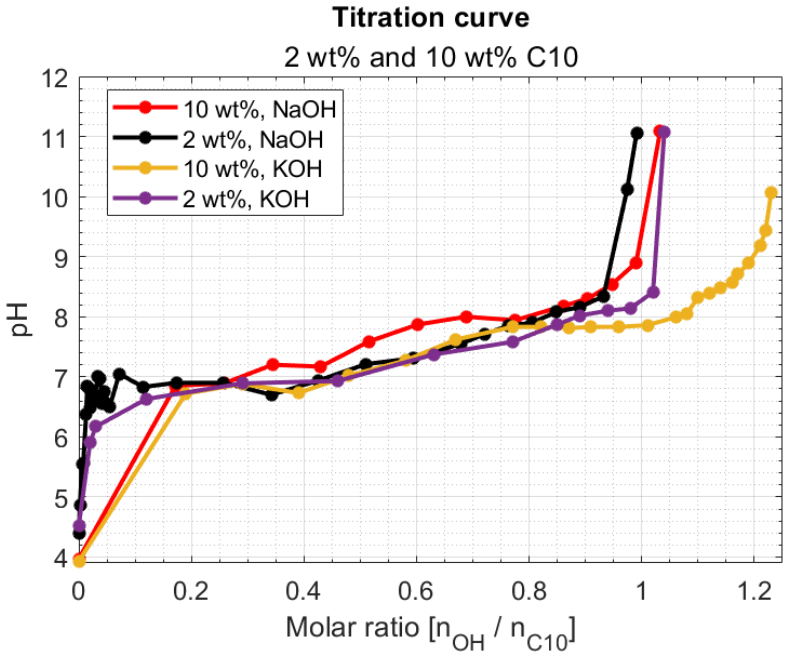

Figure 4.3: Titration curves of C10 acid in 2 and 10 wt%, titrated with NaOH and KOH.

The surfactants were characterized in a wide concentration range, 0.5 to 10%, in terms of visual inspection, DLS and SAXS, to evaluate the shape and size of the surfactant aggregates. The samples were characterized in a NaCl 0.525 wt% water solution. This is to have a comparable solvent to the mixed systems. The pH values of the samples are presented in Table 4.1.

Table 4.1: pH values (± pH 0.05) of the 10-0.5 wt% NaC10 and KC10 in water solutions, including 0.525 wt% NaCl.

C10-salt [wt%]	pH (NaC10)	pH (KC10)
10	9.22	8.52
5	9.14	8.43
2	8.67	8.11
1	7.89	7.58
0.5	7.53	-

Figures 4.4 and 4.5 presents the results of the DLS for NaC10 and KC10, respectively. In the DLS characterization results, there are peaks at 2-3 nm and above 10 nm. The peaks related to smaller sizes indicate the size of the aggregates, compatible with the size of micelles. This makes sense since the surfactant concentrations here are above CMC, around 86 mM or 1.5 wt % for NaC10 and similar for KC10. Since the ionic strength of the system is significant, the CMC is slightly decreased. Its signal strength decreases as the surfactant concentration decreases since the amount of surfactant in the sample is less, see Figure 4.4. The surfactant moves freely in the bulk or migrates towards the surface. Overall, the size of the aggregates decreases with the surfactant concentration, which is often observed for interactions between particles. The peaks for samples with surfactant concentrations below CMC do not form micellar structures. Therefore, it is difficult to determine if the observed peaks at the low surfactant concentrations originate from the surfactants that have been solubilized or contaminations.

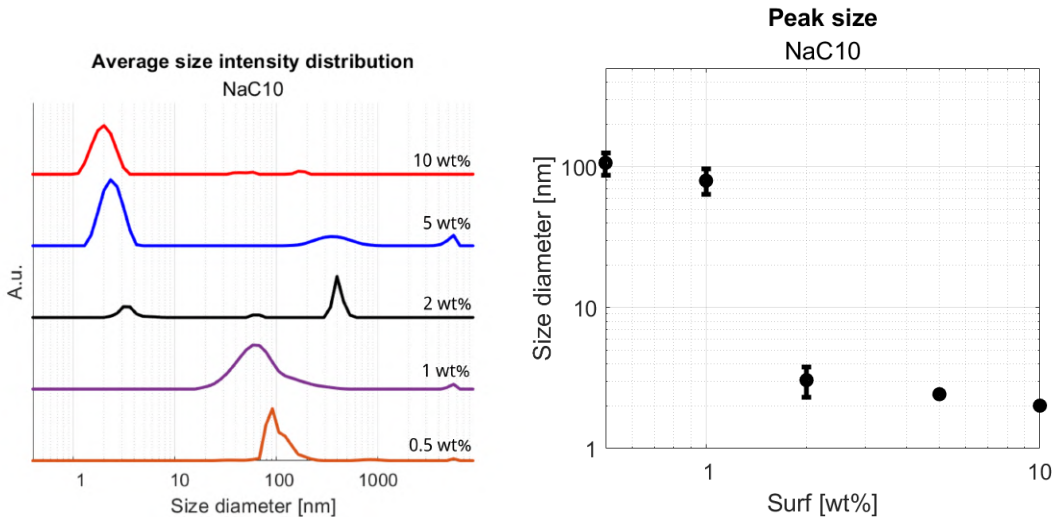

Figure 4.4: NaC10 DLS results for the concentration interval 10-0.5 wt%. (a) The average intensity size distribution results (b) The average size of the the largest population, the error bars are the standard deviation of the averaging.

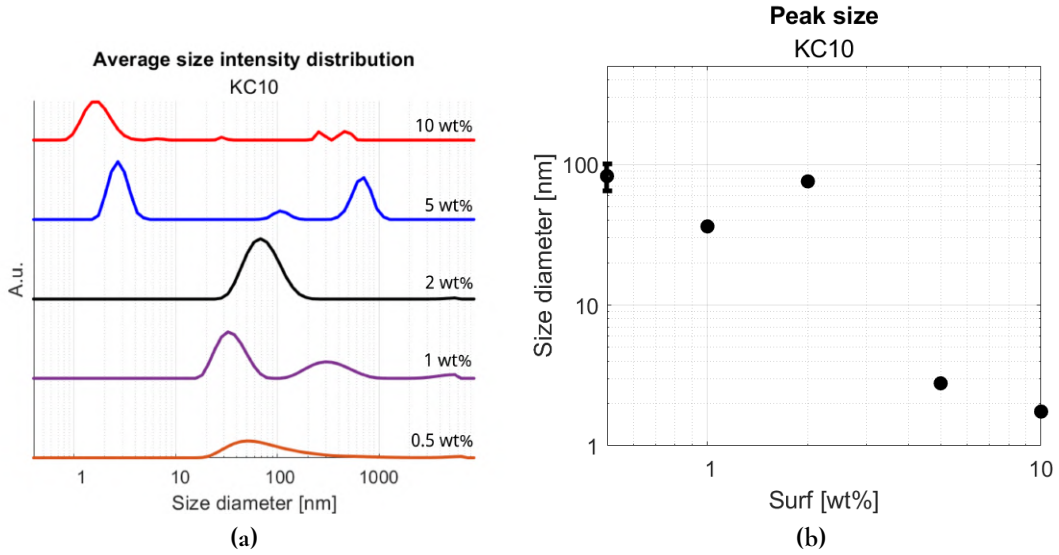

Figure 4.5: KC10 DLS results for the concentration interval 10-0.5 wt%. (a) The average intensity size distribution results (b) The average size of the largest population with error bars for standard deviation error of the averaging.

The SAXS characterization was performed on samples with a high surfactant concentration to allow for a high signal-to-noise ratio. SAXS was executed on selected samples. NaC10 was measured over the concentration range 1 to 10 wt% and 10 wt% for the KC10. The measured and treated SAXS data for NaC10 is presented in Figure 4.6 and data for NaC10 and KC10 at 10 wt% in Figure 4.7.

Figure 4.6 presents the SAXS patterns for NaC10 concentrations 1 to 10 wt%. These SAXS patterns, except for the 1 wt%, are characterized by a strong signal with the shape of a Gaussian peak, the maximum intensity of the peak at $q \approx 0.18$ Å^{-1}. Furthermore, the signal strength of this peak decreases with the surfactant concentration. The signal maximum corresponds to a repeating distance of 35 Å, which is compatible with the size of micelles. The average length of a surfactant molecule is usually 10-20 Å, so the peak corresponds to roughly two surfactant molecules in size. There are two hypotheses for the origin of this peak: periodicity between core to core micellar distance (inter-micellar characteristic spacing) or difference between the electron density of the core and the shell of the micelle.

The second one is the correct hypothesis in this case since the intensity maximum of the peak does not shift with concentration. Moreover, if it arises from a periodicity, the distance between the micellar cores would increase as the surfactant concentration decreases. This would result in a shift for the centrum of the peak to slightly smaller q-values.

Figure 4.7 compares the SAXS pattern for NaC10 and KC10 at the concentration 10 wt%. Both patterns exhibit a strong signal from a Gaussian peak that originates from the electron density profiles of the micelles. In this case, the curves are slightly shifted relative to each other, and the intensities are different at the same surfactant concentration. The NaC10 signal peak is centred around $q = 0.18$ Å^{-1} corresponding to 35 Å and the KC10 peak maximum is at $q = 0.17$ Å^{-1} corresponding to 37 Å. The peak for KC10 is centred at a slightly larger size than NaC10. Since the surfactant peak originates from the electron density profile of the

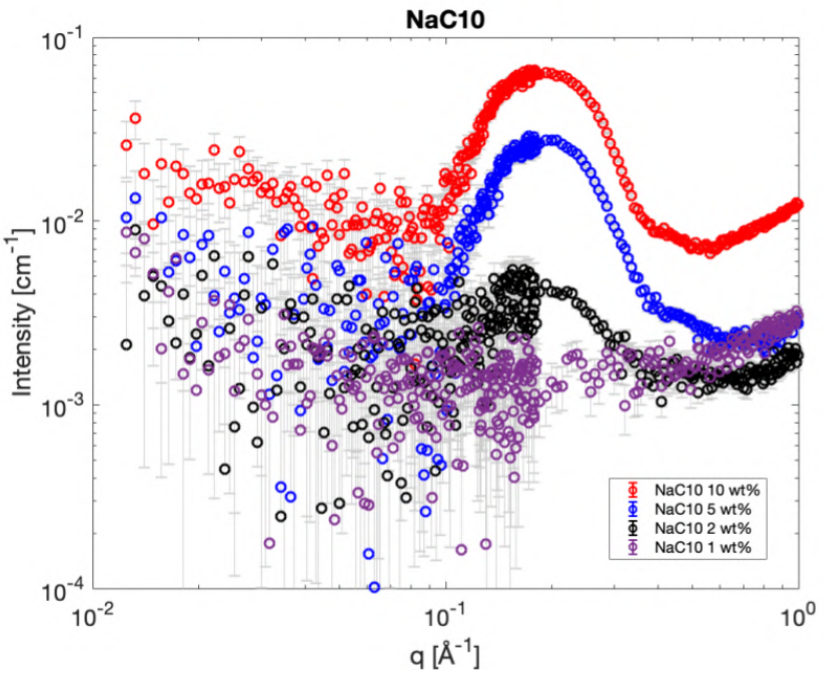

Figure 4.6: SAXS patterns for NaC10 concentration 1-10 wt%

surfactant, different counter ions result in different profiles. Potassium is a heavier element than sodium, so its electron density should be slightly more spread and coherent with the curves. The different counter ions can also explain the difference in intensity. The difference in electron density between the micelles can make one of the samples more detectable than the other, which would affect the intensity of the signals detected.

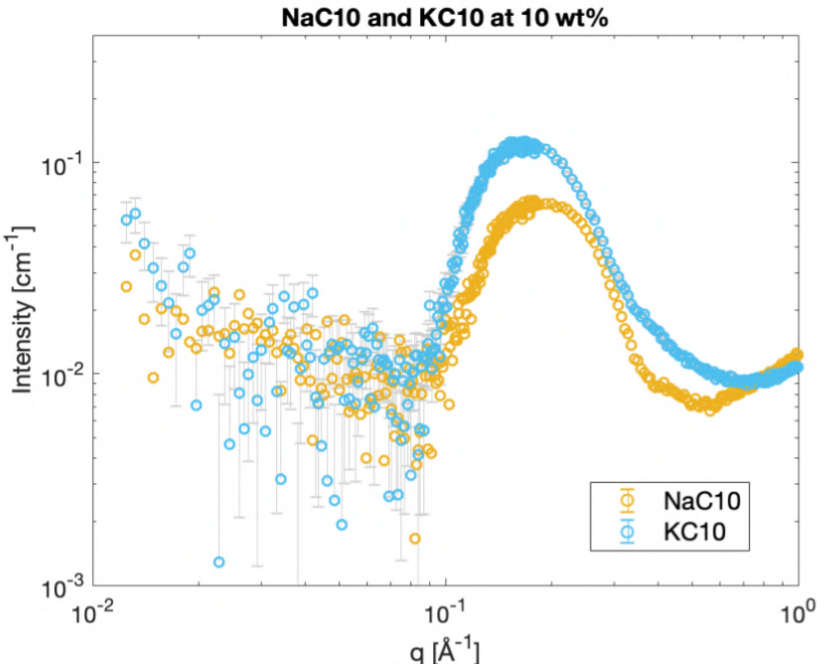

Figure 4.7: SAXS patterns for NaC10 and KC10 at 10 wt%.

The fitting of NaC10 and KC10 at 10 wt% with the core-shell model in SasView [27] is presented in Figure 4.8. The results of the fit are summarized in Table 4.2, where the radius, thickness and scattering length densities are presented. Comparing the data from the two fits, the core radius is the same for both salts and is 9 Å. On the other hand, the thickness of the shell is different and is 16 for NaC10 and 20 for KC10. This is compatible with the counterion effect mentioned earlier that potassium is a larger and heavier atom with a more spread out electron density, which results in a thicker shell structure of the micelles [30].

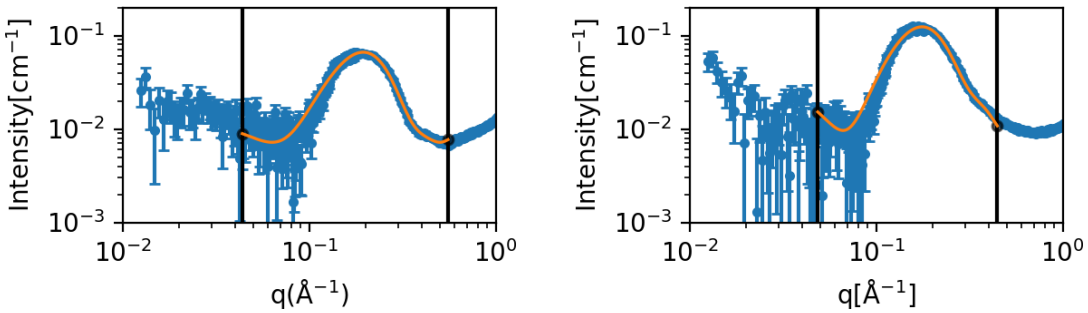

(a) **(b)**

Figure 4.8: The surfactant salts SAXS patterns at the concentration 10 wt% together with the theoretical core-shell sphere structures modelled in SasView: (a) NaC10 and (b) KC10 at the concentration 10 wt%.

Table 4.2: Summary of the theoretical fitting done in SasView with core shell sphere model for NaC10 and KC10 at the concentration 10 wt%. The data extracted from the fit was the radius of the core and thickness of the shell. ρ is the scattering length density and $\Gamma istheradiusorthickness, withc= core, s= shell, sol= solvent.$

Surfactant salt	r_c [Å]	r_s [Å]	ρ_c 10^{-6}[Å^{-2}]	ρ_s 10^{-6}[Å^{-2}2]	ρ_{sol} 10^{-6}[Å^{-2}]
NaC10	9	16	6.79	9.57	9.40
KC10	9	20	6.22	9.55	9.40

4.1.2 Size and shape of studied cationic inulin derivatives

The size characterization method used on the surfactants was applied to Q350 and Q680. The polymers were studied in a water solution at concentrations of 0.5 and 2 wt%, including a background salinity of 0.525 wt% NaCl. The DLS results for Q350 and Q680 are presented in Figure 4.9 at the concentrations 0.5 and 2 wt%. The intensity curves show that the largest population is distributed around 3 nm for Q350 and Q680 at both concentrations. The main difference in property between the polymers is the charge density, which does not seem to affect the polymers' size. Moreover, in Figure 4.9 there are minor peaks present for all signals in the range 100-1000 nm, and additionally, a peak above 1000 nm for the samples Q680 0.5 wt% and Q350 2 wt%. Contaminations and impurities probably cause peaks in size range of 100-1000 nm and artefacts for signals above 1000 nm.

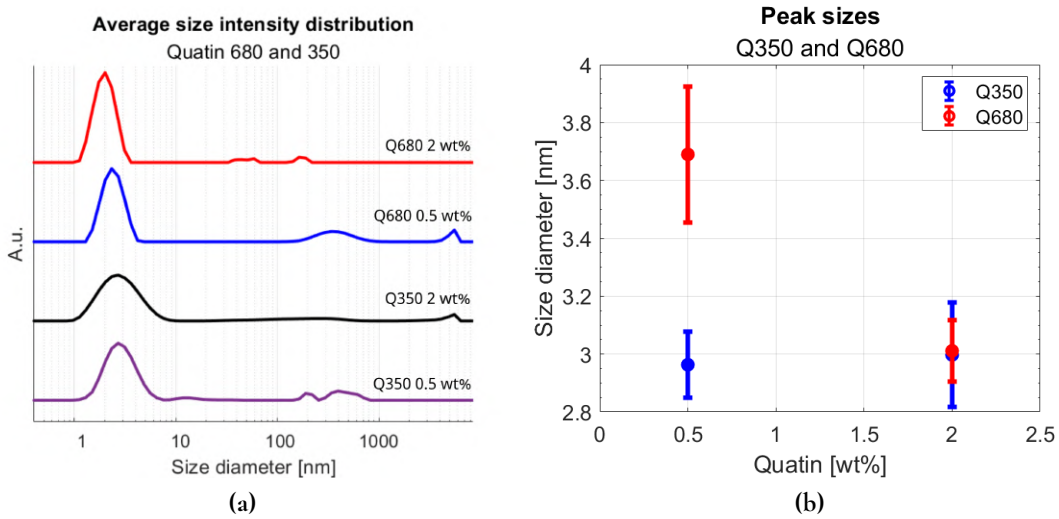

Figure 4.9: DLS results for Quatin 350 and 680 at concentrations 0.5 and 2.0 w% (a) The average size distribution by intensity for Q350 and Q680 (b) The average size of the largest population, the error bars are the standard deviation of the experiment.

The SAXS patterns were collected for the polymer solutions, Q350 and Q680, at concentrations 0.5 and 2 wt% are presented in Figure 4.10 The curves collected for the polymers look similar. More specifically, plots with the same concentration of Q350 and Q680 reach the same plateau value at low q, and the slopes of the curves from q =0.1 to large q-values are similar.

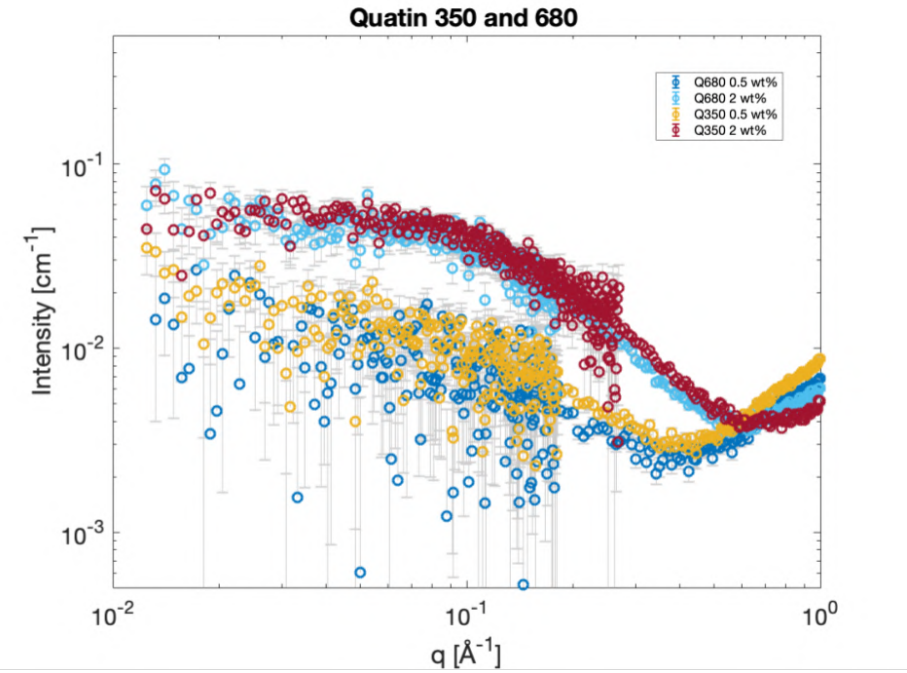

Figure 4.10: SAXS patterns for QUATIN® 350 and 680 at concentrations 0.5 and 2 w%.

The SAXS pattern was fitted with the Debye function, see Equation 3.1 in the method section. The fitting was performed to determine the polymer chains' R_g. This fitting is presented for all curves in Figure 4.11, with the approximated R_g included. The approximated radii are within 9-12 Å. The calculated R_g for the concentration 2 wt% was smaller than for the 0.5 wt%, with a difference of 2 Å between the concentrations, for both polymers. The calculated radius of gyration is small in comparison to conventional polymers and is compatible with inulin, the polymer backbone to QUATIN. Inulin has been reported to have a degree of polymerisation between 2-60 monomers[11].

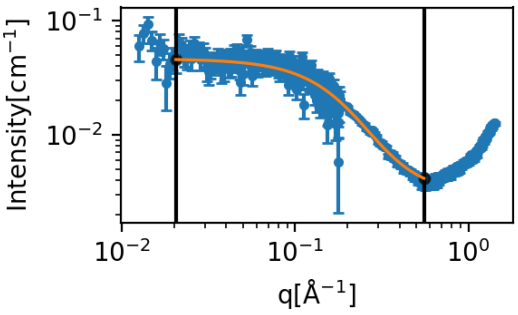

(a) Q680 2 wt%, radius of gyration determined to 10 Å.

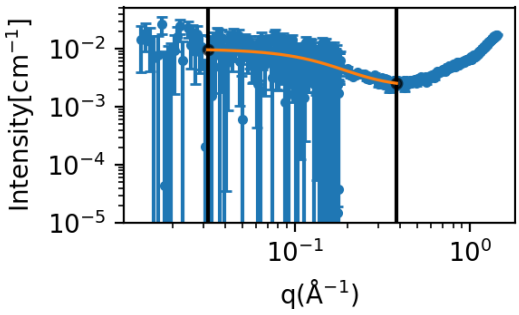

(b) Q680 0.5 wt%, radius of gyration determined to 12 Å.

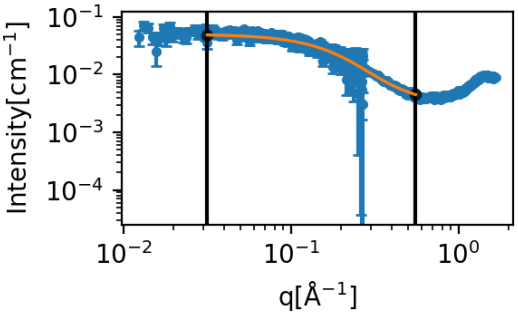

(c) Q350 2 wt%, radius of gyration determined to 9 Å

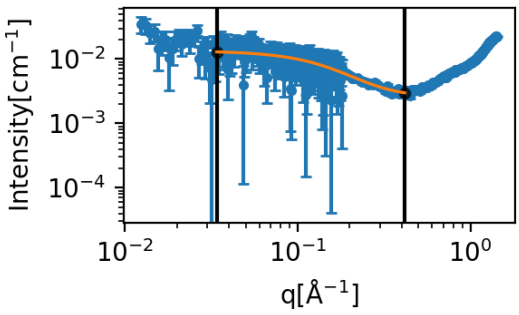

(d) Q350 0.5 wt%, radius of gyration determined to 11 Å

Figure 4.11: Series presenting the SAXS patterns for Q350 and Q680 at concentrations 0.5 and 2 wt% together with the theoretical Gaussian chain model for these patterns. The calculation was preformed in the software SasView using the Debye function, using the characteristic exponent for Gaussian chains. The two black vertical lines in the figures represents the q range which the fitting covered.

4.2 Chapter 2 | Mixed systems and bulk studies

In this chapter, mixed systems containing surfactant and polymer were analyzed in a wide composition range to identify possible coacervate formation windows and identify what parameters are crucial for this formation to occur. In particular the ranges 0.1-10 wt% C10-salt and 0.5-2 wt% polymer were investigated. These concentrations were used because they are quite usual for formulated products.

Prepared in this thesis are the following surfactant-polymer systems:

- NaC10-Q350
- NaC10-Q680
- KC10-Q350
- KC10-Q680
- NaC10-N-Hance

4.2.1 Mixed systems with cationic inulin derivatives

Dilution series were performed to explore a wide composition range for each combination. Such dilutions were performed with either a polymer dilution solution to change the surfactant/polymer ratio or a water dilution solution to dilute both ingredients equally. For the dilutions performed with QUATIN® polymers, the pH decreases because the polymer stock solution has a low pH (5), and that becomes more and more predominant as the samples are diluted further.

For each combination of the Na/KC10-QUATIN® dilution series, sample matrices were made, shown in Figure 4.12. The matrices were populated according to visual inspection of the samples. The visual appearance of the samples was observed right after preparation. It was observed that the majority of the samples were visually clear and had a water-like viscosity. On the other hand, some samples were turbid after preparation (see Figure 4.13). In each graph, the line represents (S/P) = 1, i.e. charge neutrality, as introduced in the background section. Charge neutrality is usually considered an essential condition when studying coacervate formation, as they often are observed at this point. However, it is not the only criterion, as some other parameters might play an important role.

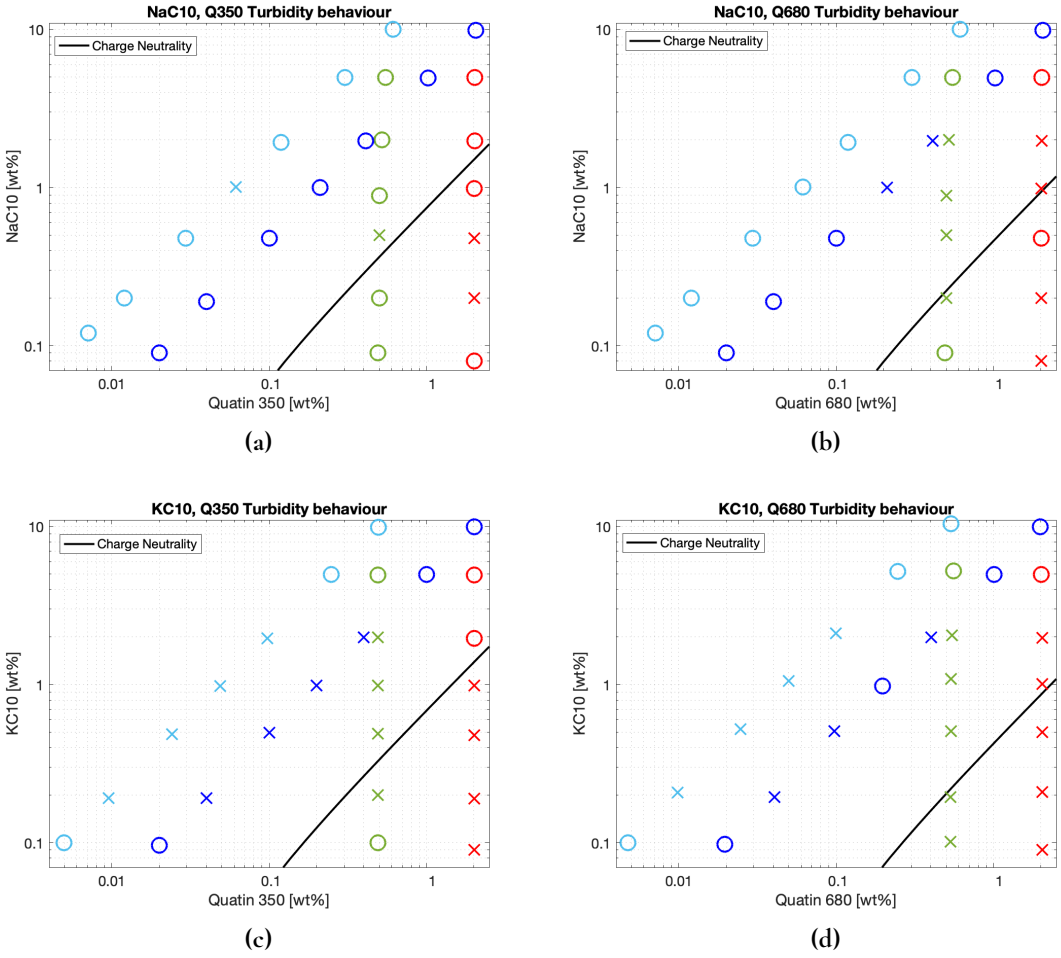

Figure 4.12: Sample matrices for the different surfactant-polymer systems: NaC10 (top), KC10 (bottom) with polymers Q350 (left) and Q680 (right). Samples that has been marked with a cross 'X' was classified as turbid meanwhile circles 'O' were clear samples. The line is (S/P) = 1, i.e. charge neutrality, for each system.

This section will focus on the NaC10-Q680 2 wt% polymer- and water dilution series. The systems were characterized in terms of visual appearance, size and shape of the aggregates via DLS and SAXS. There are two major reasons these two series were focused on in this thesis. Firstly, Na is a commonly studied ion. Secondly, a higher polymer concentration gave better detection and quality in the measurements, which is easier to interpret. In the Appendix section, the visual appearance of the other dilution series is presented.

Characterization of NaC10 Q680 2 wt% dilution series

The first series to be introduced is the NaC10, with the concentration range 0.1-10 wt%, combined with polymer Q680 2 wt%, see Figure 4.13 that shows the visual appearance for samples 0.1-5wt% in this series. Turbidity was observed for samples 0.1, 0.2, 1 and 2 wt% NaC10. On the other hand, 0.5, 5 and 10 wt% were clear. All samples were water-like in viscosity. Table 4.3 shows the pH and (S/P) charge ratio values of the series of NaC10-Q680.

The pH range for the dilution series is 9 at high and 6 at low concentrations, see Table 4.3. Additionally, the (S/P) ratio also decreases with the surfactant concentration. Therefore, a competing effect between the (S/P) ratio and pH might give rise to this turbidity. In later experiments, the pH parameter was kept constant to study one of the effects. Furthermore, the turbidity at low pH values might not be related to coacervate formation but instead that the surfactant becomes insoluble.

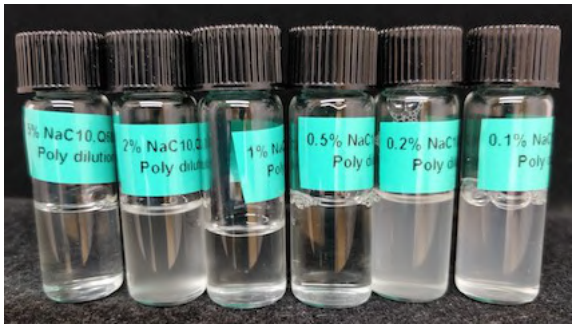

Figure 4.13: Visual appearance of the 5, 2, 1, 0.5, 0.2 and 0.1 wt% NaC10 -Q680 2 wt% series.

Table 4.3: pH values (± pH 0.05) and the (S/P) charge ratio values for the series NaC10- Q680 2 wt%.'*' = turbid samples, '**' = highly turbid sample.

		Q680 2 wt%	
		pH	**(S/P)**
NaC10 wt%	5	9.06	4.59
	2	**8.7****	**1.85**
	1	**8.19****	**0.95**
	0.5	7.48	0.46
	0.2	**6.8****	**0.19**
	0.1	**6.32***	**0.09**

The particle size distribution profiles obtained via DLS for this series are presented in Figure 4.14, as well as the largest population size for all the different concentrations. At higher concentrations of 5 to 10 wt%, the peaks originate from micellar structures and possibly polymers. The 10 wt% has two populations that can be distinguished, one with an average size of 3 nm and the other with 10 nm. Meanwhile, the 5 wt% only has one population present at the size 9 nm. For the turbid samples 1 to 2 wt%, there might be multiple scattering events, or the correlation function decay time was too long for the DLS instrument to analyze. Therefore, it is probable that the peaks for these signals are not related to the sample and are instead artefacts caused by the issues mentioned above. Below 1 wt% NaC10, the aggregate size increases as the NaC10 concentration decreases. The cause for this is that the surfactant becomes insoluble at these low pH values, see Table 4.3, and forms large aggregates.

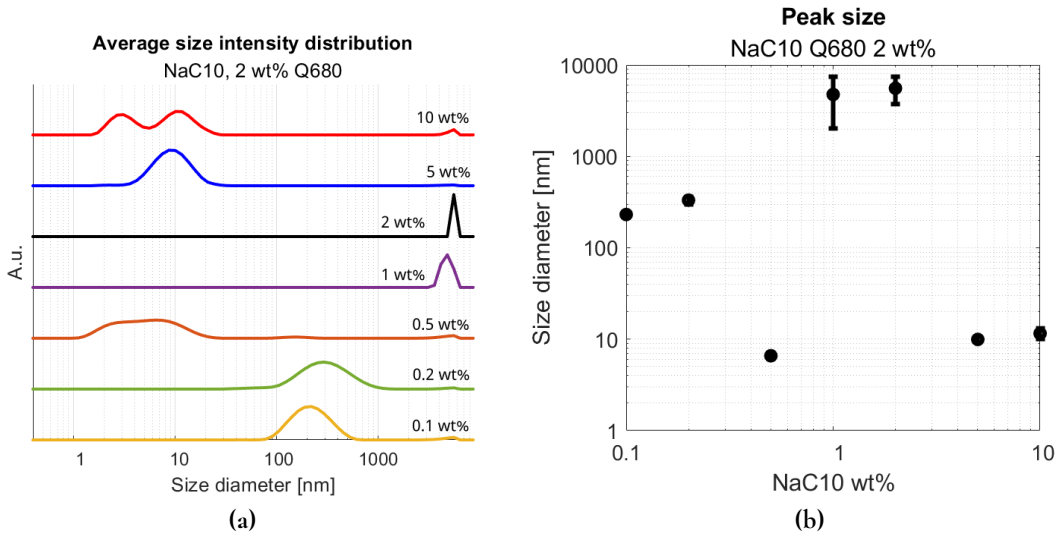

Figure 4.14: DLS results for NaC10-Q680 2 wt% polymer dilution (a) The average size distribution by intensity for Q350 and Q680 (b) The average size of the largest population, the error bars are the standard deviation of the experiment.

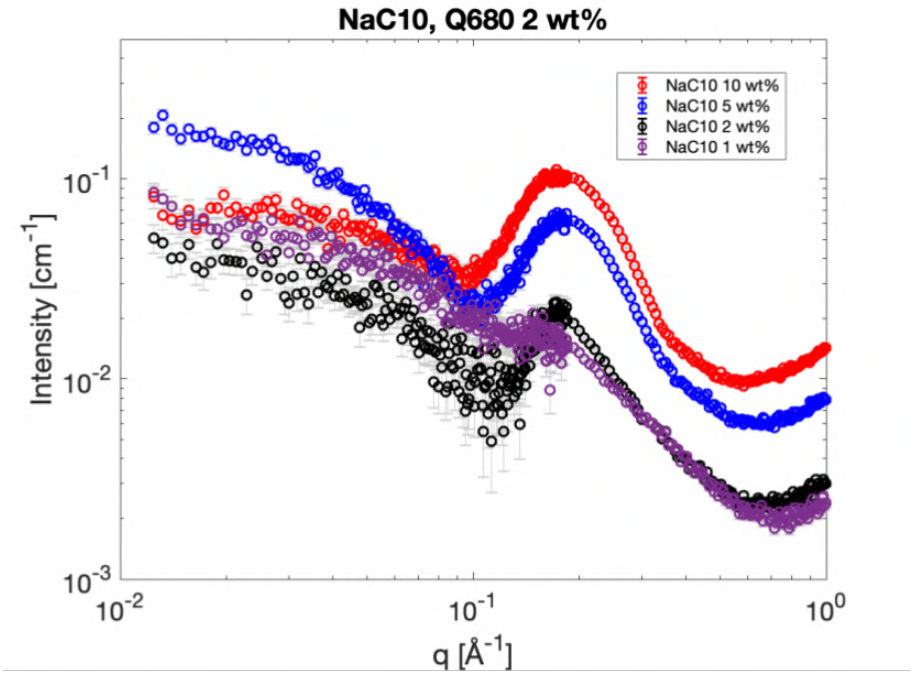

Figure 4.15: SAXS patterns for 1 to 10 wt% for the NaC10- Q680 2 wt% polymer dilution series.

The SAXS pattern collected in the concentration range 1 to 10 wt% for the mixed system NaC10-Q680 2 wt% is presented in Figure 4.15. The SAXS pattern displays features related to the surfactant and polymer. More specifically, the Gaussian peak centred around $q = 0.18$ Å $^{-}1$ decreases in intensity as the surfactant concentration is lowered. It is related to the electron

density of the micelles. The Gaussian peak is more pronounced for the 2 to 10 wt% curves, but some minor features can still be observed for the 1 wt%. If the corresponding NaC10 1 wt% curve without any polymer, see Figure 4.6 is compared, this feature cannot be seen. This is because it is below the CMC. Suggesting that the polymer allows the surfactant to form premicellar aggregates, and the sample is above CAC. Additionally, the exponential decay in intensity from $q = 0.1$ Å $^{-1}$ corresponds to the polymer. However, the SAXS pattern alters in these features depending on the surfactant concentration. As the surfactant concentration changes, so does the (S/P) ratio because the polymer concentration is constant throughout the series. Such modification would be the 5 wt% signal, (S/P)= 4.59, which levels out at higher intensity for low q-values and has a steeper slope to the surfactant peak. This strongly suggests some interaction between surfactant-polymer and some degree of co-assembly to complexes in this size range. If no phenomena occurred, the signal would level out on the same intensity as the other curves.

Characterization of NaC10, Q680 2 wt% water dilution series

In the water dilution series, samples were prepared by diluting the 10 wt% NaC10-Q680 2 wt% system with water, thus not changing the surfactant-polymer ratio throughout the series. In Table 4.4 the pH and (S/P) ratio values are presented. The pH range for the series is in the range of 7.5-9, being at ≈ 9 for the more concentrated samples and decreasing to 7.5 for the larger dilutions, which is a narrower pH range than the series above, polymer dilution. This is because, in the previous series, there was a polymer dilution with a stock polymer diluent of pH 5, which was added, whereas this series is diluted with solely water. Therefore, the pH is not lowered by the polymer and does not change a lot. Thus, the NaC10 is not protonated and remains soluble in the solution.

Table 4.4: pH values (± pH 0.05) and (S/P) values for the samples in the NaC10-Q680 water dilution series. '*' = turbid sample.

		Q680 2	
		pH	**(S/P)**
NaC10 wt%	10	-	9.65
	5	9.16	
	2	**8.73****	
	1	8.15	
	0.5	7.98	
	0.2	8.03	
	0.1	8.23	

The particle size distribution profiles obtained via DLS for NaC10-Q680 2wt% water dilution series are presented in Figure 4.16a, together with a summary of the average size of the largest population. The DLS data shows the same trend for higher concentration samples 10 and 5 wt% and the turbid samples as in NaC10 Q680 2 wt% polymer dilution. However, for the low NaC10 concentrations, the samples are very diluted, so the signal from the polymer or surfactant is no longer distinguishable from the background noise. Dust or other contaminations most likely cause the peaks at larger sizes at these lower concentrations.

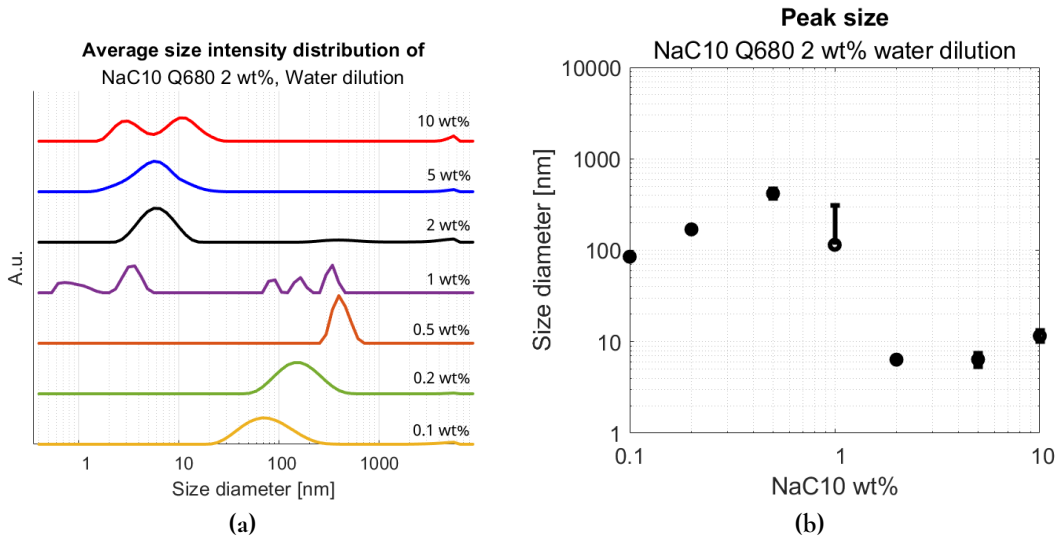

Figure 4.16: DLS resulsts for 0.1-5 wt% NaC10-Q680 2 wt% water dilution series. (a) The average intensity size distribution results (b) The average size of the highest mean peak intensity with error bars for standard deviation error of the averaging.

The SAXS patterns collected for the water dilution series are presented in Figure 4.17. These patterns exhibit features both from the surfactant and polymer. The feature corresponding to the micelles' electron density is the Gaussian peak centred at $q \approx 18$ Å^{-1}. The peak is present for concentrations 2 to 10 wt% that are above the CMC. The peak decreases in intensity as the surfactant concentrations are lowered. The features corresponding to the polymer are those at low q, the plateau, and the signal's slope to the Gaussian peak. The intensity of the plateau decreases with the surfactant concentration, except for the 5 wt% pattern that has an intensity similar to 10 wt% curve. The behaviour for the features related to the surfactant at high q could be seen for the corresponding polymer dilution, which was discussed earlier. However, the polymer features are different compared to the polymer dilution. This is because both the polymer and surfactant are diluted in this series, so the (S/P) ratio is constant at 9.65. Therefore, the polymer plateau decreases in intensity with further dilution.

The 5 wt% curve has an intensity similar to the 10 wt% at low q-values. Indicating that interactions occur, this co-assembly could also be seen for the same surfactant concentration in the corresponding polymer dilution. The (S/P) ratio for the water dilution is 9.46 and 4.59 for the corresponding polymer dilution. The (S/P) ratio in the water dilution is twice as large as the polymer dilution series. Suggesting that the co-assembly is probably not related to the (S/P) ratio of the samples but instead some other phenomena that happen at this surfactant concentration.

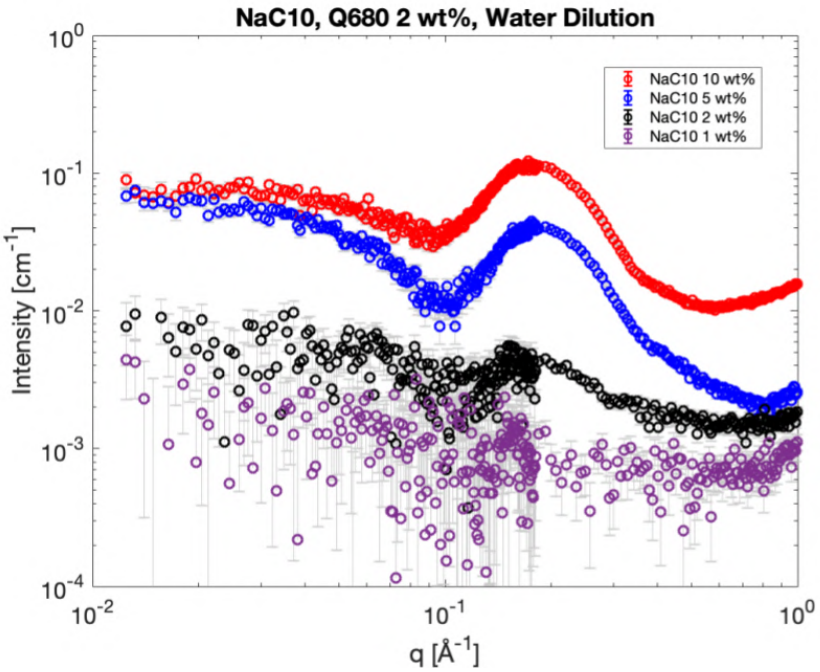

Figure 4.17: SAXS patterns for 10, 5, 2 and 1 wt% NaC10-Q680 2 wt% water dilution series.

4.2.2 Effect of pH

In the previous series in the sections above, a variation of the pH with varying degree of dilutions was observed, especially for the polymer dilution series. When moving from high to low wt% NaC10, the pH dropped from 9 to 7, or even pH 6, see Table 4.3. Additionally, this trend could also be seen in the KC10 dilution series. As mentioned before, there is a strong correlation between the solubility of the surfactant and the pH, therefore this is a parameter to be controlled for observing the behaviour of the systems. Therefore, selected series were adjusted to approximately pH 9 by drop-wise addition of base, NaOH or KOH. An example of the visual difference can be seen in the images of the series NaC10-Q680 2 wt% in Figure B.2. Before adjustment of pH, turbidity occurred for concentrations 0.1, 0.2, 1 and 2 wt% NaC10. After pH adjustments, the turbidity for samples 1 and 2 wt% NaC10 was still present, whereas the samples with lower NaC10 concentration became clear. The Appendix provides additional examples of this. The lower concentrations became clear after pH adjustments confirmed that the pH was too low for the surfactant to be soluble, which was suspected. Since the pH was below or approximately the pKa of the surfactant, the surfactants remain unprotonated and therefore insoluble.

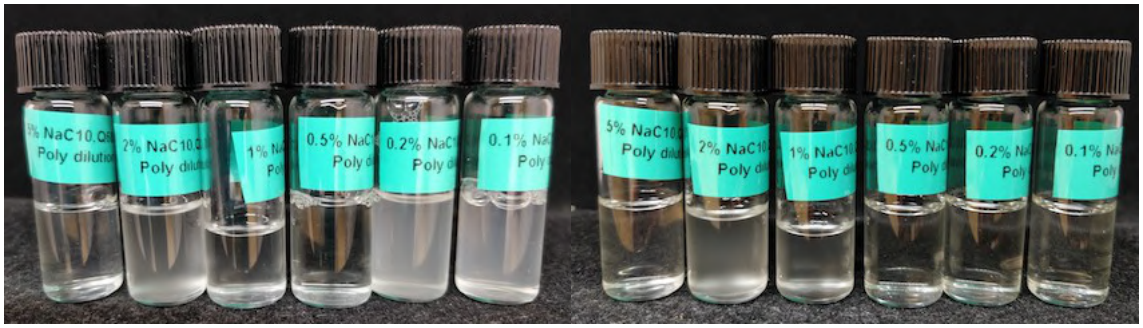

(a) Before pH adjustment **(b)** After pH adjustment

Figure 4.18: Visual appearance of the polymer dilution series, 5, 2, 1, 0.5, 0.2 and 0.1 wt% NaC10- Q680 2 wt% series. The samples were adjusted to pH 9. The lower concentrations 0.1-0.5 wt% NaC10 lost turbidity after pH adjustment.

4.2.3 Controlling pH with a buffer

An alternative way of keeping constant pH around 9 is using a buffer. This is preferred from a practical point of view, as it does not require manual pH adjustment for each sample. The buffer selected to reach pH 9 was Tris 20 mM, which was added to each sample. The NaC10-Q680 mixture was chosen to be further investigated to understand if the systems obtained with and without buffer are comparable. A sample matrix was created for this system, see Figure 4.19. Additionally, the sample matrix was populated with the visual appearance of the samples after they were allowed to rest for three days and then sonicated. Here an additional polymer dilution concentration was added, 0.2 wt%. This new lower polymer concentration was added to fill the matrix and increase the investigated area where possible coacervate formation might occur. Moreover, the series that will be studied more in detail is polymer dilution at 2 wt% Q680 (red in the matrix) and water dilution at 2 wt% (blue in the matrix). Moreover, all of the other series exhibited similar behaviour to these.

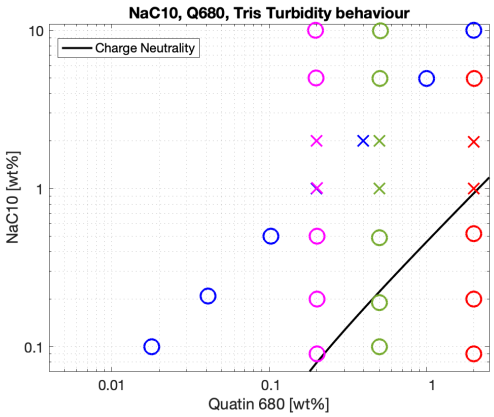

Figure 4.19: NaC10 Q680 Tris sample matrix, the blue line corresponds to (S/P) = 1. Circles 'O' are samples classified as clear and crosses 'X' represent turbid samples.

Before investigating the polymer-surfactant mixture, the single ingredients were also studied with SAXS to see if Tris affected their aggregation behaviour. In Figures 4.20a the SAXS patterns of a) NaC10 10 wt% and b) Q680 2 and 0.5 wt% with and without Tris are presented. The NaC10 curves in Figure 4.20a look very similar, but one has a deeper minimum at $q \approx 0.08 \text{Å}^{-}1$. The R_g is calculated with the volume excluded model in the software SasView, and it was determined to be 9 Å, for Q680 2 wt% with 20 mM Tris. The R_g for the same polymer concentration in Figure 4.11 without Tris was determined to be 10 Å, which is similar in size—indicating that Tris does not have an impact on the polymers' aggregate size.

The measurements in Figures 4.23 (a) and (b) for samples with and without Tris were done at different places on the capillary, which had different thicknesses. This gives a difference in intensity at high q-values. More specifically, measurements on samples without Tris were performed at the neck of the capillary, which is thicker than the main body where all other measurements were performed. The thickness of the capillary neck increases the intensity of the signal at high q and is very irregular in thickness, making it very difficult to make a proper background subtraction, especially in the high q-region.

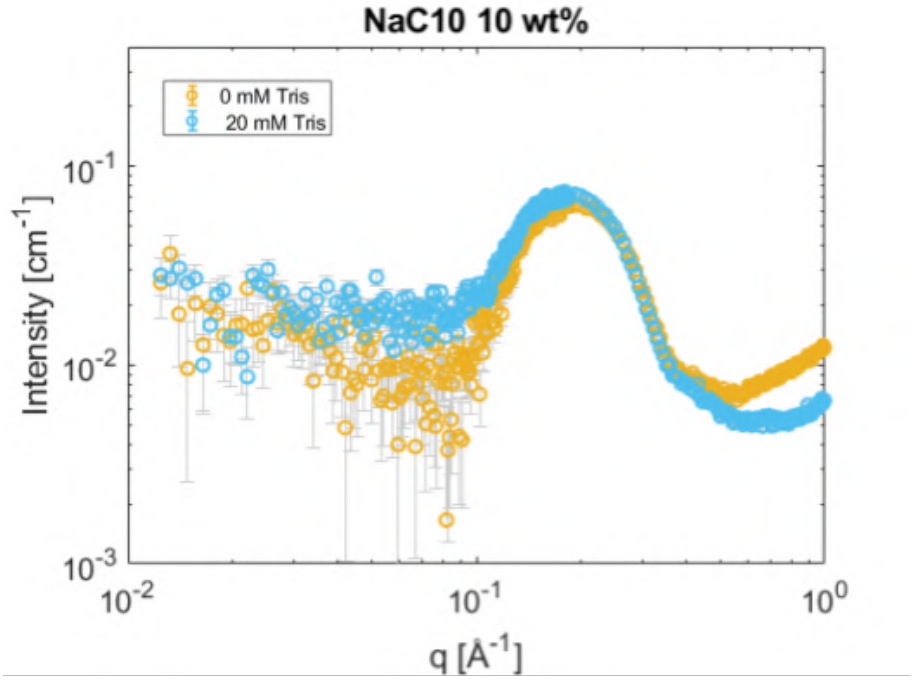

(a)

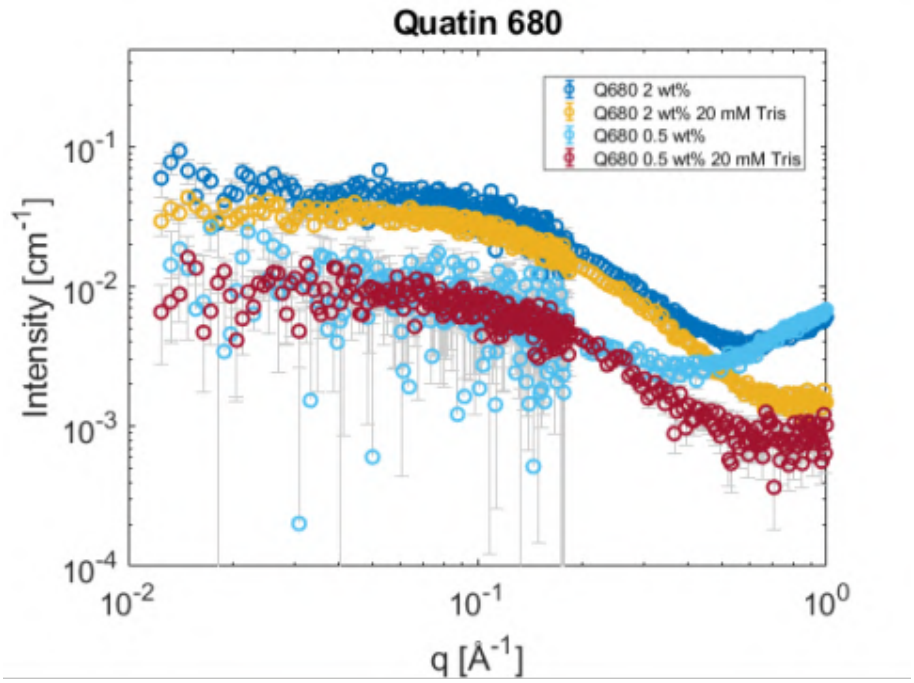

(b)

Figure 4.20: SAXS patterns of NaC10 and Quatin 680 with and without Tris 20 mM (a) NaC10 at 10 wt%. (b) Q680 at 0.5 and 2 wt%

Characterization of NaC10-Q680 2 wt% with Tris dilution series

In Figure 4.21 the visual appearance of the NaC10-Q680 2 wt% polymer dilution series with Tris 20 mM is presented. The visual appearance of the samples in this series is comparable with the one of the pH adjusted one, see Figure C.3c, in terms of turbidity and viscosity. The pH and (S/P) ratio for this Tris series are presented in Table 4.5. Upon visual inspection of the images mentioned earlier, the addition of Tris does not appear to have any other effects than keeping the pH constant at around 9 for the series.

The samples of concentrations 1 and 2 wt% NaC10 exhibited turbidity immediately after preparation and were water-like in viscosity like the other samples in the series. After three days, certainly for the 2 wt% sample, clear phase separation could be observed between a viscous gel phase and a transparent water-like phase. A timeline of the visual appearances is presented in Figure 4.24 and the phase separation is shown in Figure 4.25. This phase separation will be studied more in depth later in the section.

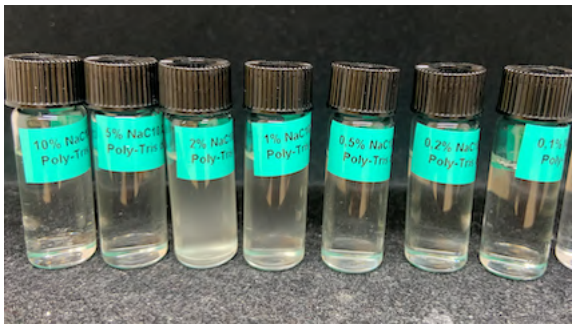

Figure 4.21: Visual appearance of the 10, 5, 2, 1, 0.5, 0.2 and 0.1 wt% NaC10-Q680 2 wt% Tris series.

Table 4.5: (S/P) values and pH values (± pH 0.05) three days after preparation for polymer dilution series NaC10-Q680 2 wt%.

NaC10 [wt%]	pH	(S/P)
10	9.13	9.46
5	9.11	4.68
2	**8.90****	**1.84**
1	**8.84****	**0.93**
0.5	8.84	0.48
0.2	8.88	0.19
0.1	8.93	0.08

The DLS data are presented in Figure 4.22 for the dilution series. For the higher concentrations samples, 5 and 10 wt%, the largest population sizes are observed between 1-12 nm. This size range is compatible with the polymers and micelles in sizes 2-10 nm measured in the single ingredient section. The trend at higher surfactant concentrations could also be seen in the previous DLS measurements on the same series without Tris, see Figure series 4.14.

The samples of intermediate concentrations, 1 and 2 wt%, mainly have signals at sizes above 100 nm. These samples are too turbid to observe anything significant. The signals detected are probable to be artefacts.

For the lower concentrations, 0.5 wt% and lower, mainly one population is observed at smaller sizes, approximately 3 nm. The polymer gives these signals. Since these samples have a concentration below CMC, micelles cannot be formed. Instead, the surfactant floats in the bulk or migrates to the surface. Therefore it is no longer detectable. Additionally, this trend was seen for all the polymer dilutions in the Tris series. The signals at sizes above 3 nm for sample 0.5 wt% are not particularly pronounced and are probably caused by contaminations.

The DLS results for the corresponding series with and without Tris exhibited similar behaviour for the concentration range 1-10 wt%. Below 1 wt% concentration, NaC10 precipitated because the polymer decreased the pH of the samples below the surfactants pKa for the series without Tris. However, since the trends were similar above the 1 wt% concentration, the solubility of the surfactant was not an issue. Again, this suggests that Tris does not have any other effect than keeping the pH constant.

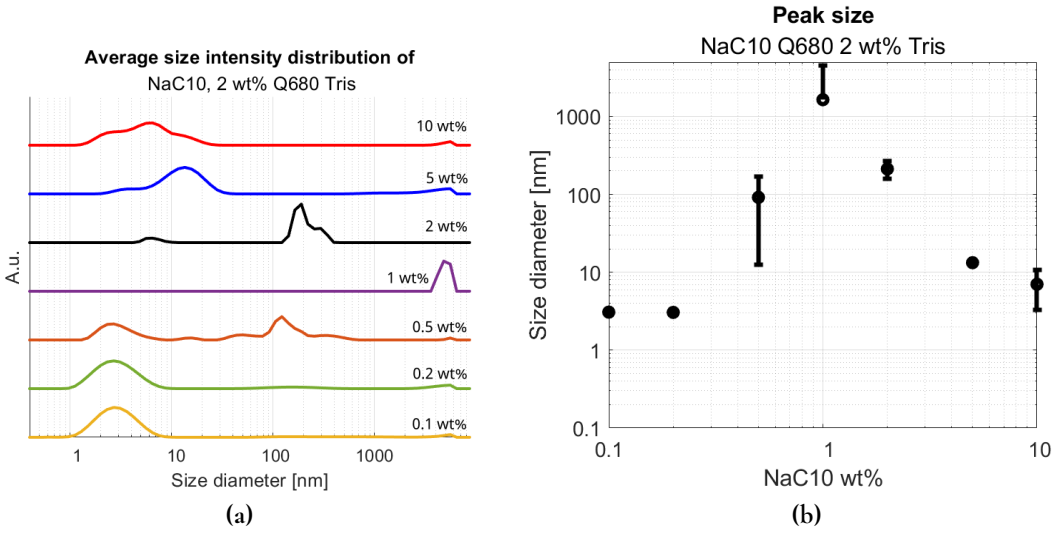

Figure 4.22: Average size distribution by intensity DLS measurements for the concentrations NaC10 0.1-10 wt% for the NaC10, Q680 2 wt% polymer dilution including Tris series. (a) The average intensity size distribution results (b) The average size of the highest mean peak intensity with error bars for standard deviation error of the averaging.

SAXS analysis on this series for concentration range 1 to 10 wt% NaC10 shows a similar trend to earlier studied series, and the patterns are presented in Figure 4.23. The key feature of the series is that the surfactant peak does not shift as the surfactant concentrations decrease, and the blue curve corresponding to the 5 wt% sample has a higher intensity at low q-values than the other curves that have the same. These features could be seen in the corresponding polymer- and water dilution series without Tris.

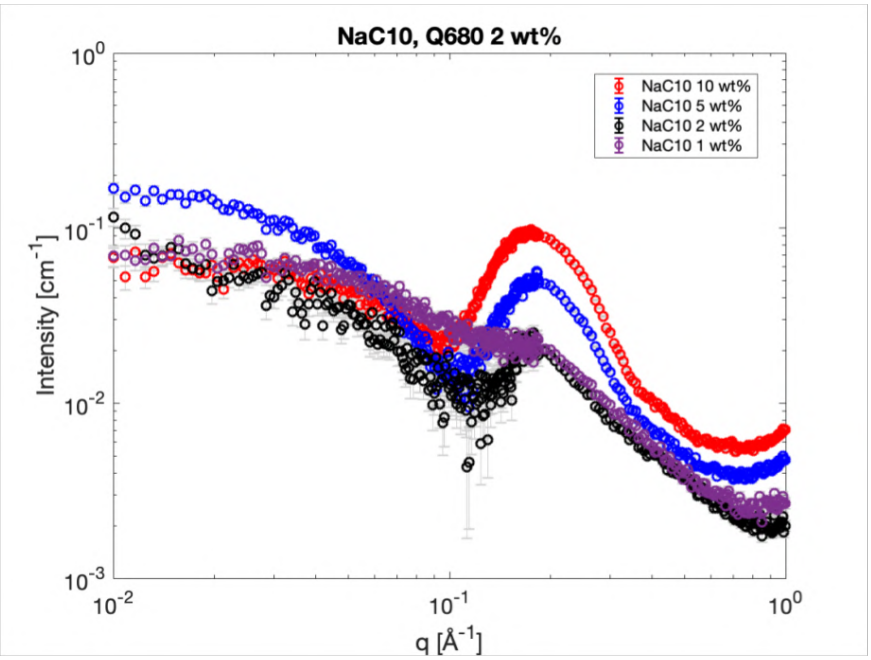

Figure 4.23: The SAXS data for the NaC10 Q680 2 wt% with 20 mM Tris.

Phase separation study of 2 wt% NaC10-Q680 2 wt% with Tris

One particularly interesting sample is 2 wt% NaC10-Q680 2 wt%. It appeared turbid immediately after preparation and phase separated within three days into two transparent phases, the bottom one exhibiting a high viscosity. Such phase separated sample could be brought back to the initial condition (turbid system) by shaking or sonication. This can be seen in Figure 4.24. Given the relatively high concentration of the two components, this was the only sample among the turbid ones where a two-phase system could be identified upon equilibration. In the other cases (e.g. sample with 1 wt% NaC10), the viscous gel phase was not easily identifiable by visual inspection since it formed small droplets that formed a homogeneous film around the vial walls. Furthermore, the separation behaviour into supernatant and a viscous gel is the definition of coacervation. This phase separation indicates that the sample is within the coacervate formation window.

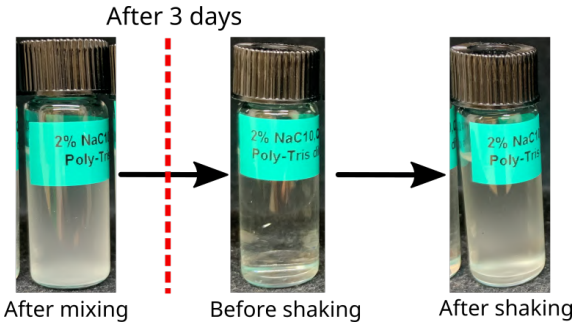

Figure 4.24: Timeline of sample NaC10 2 wt% Q680 2 wt% with 20 mM Tris.

Additionally, as the polymer concentration decreased, moving horizontally to the left in the sample matrix shown in Figure 4.19. The weighted amount of polymer which could phase separate became less, and the gel became more difficult to distinguish upon visual inspection. For example the 0.2 wt% Q680 sample, the gel phase was arranged in smaller clusters that stuck to all sides of the vial, and upon visual inspection, it could no longer be seen. Finally, the 0.2 wt% Q680 had to be sonicated in a sonic bath for the samples to display turbidity, suggesting that it becomes harder to induce microphase separation as we decrease the polymer concentration. Furthermore, smaller clusters of coacervates could be suspended in the clear non-viscous phase at lower polymer concentrations, which was not seen at higher concentrations.

The two phases were separated and analyzed separately by SAXS. The SAXS patterns of the two phases, as well as for the mixed (turbid) system, are presented in Figure 4.25. The overall intensity of the gel phase is much higher than the supernatant phase and when the phases are mixed, indicating a higher concentration of both surfactant and polymer compared to the nominal concentration of the sample. Notably, the surfactant peak for the gel phase is much sharper and more triangular than the standard Gaussian shape it has typically. The form of the peak might be caused by the high-density packing of the gel phase consisting of polymers and surfactants. The intensity is high, explained by a strong interaction between the polymer and surfactant. Hence, the gel phase gets compacted in a highly concentrated system at the bottom.

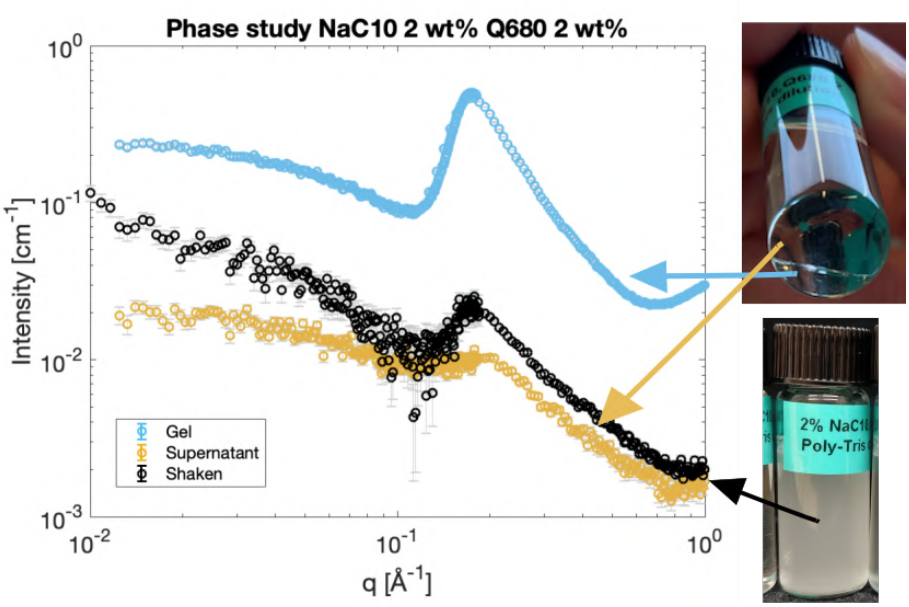

Figure 4.25: SAXS patterns of the phase separation and mixing of phases for sample NaC10 2 wt%- Q680 2 wt% with 20 mM Tris. Images of the samples are included. The q-values for the maximum of the peak from top to bottom: q = 0.17, 0.18, 0.19.

Moreover, the surfactant can adapt to fewer configurations at higher packing densities, narrowing the peak width. The surfactant peak also does not show any significant shift in q-values between the three curves. The intensity of the mixed turbid sample is in-between the intensities of the other two separated phases, which is reasonable since it is supposed to

be an average of the two. It is specifically the average weighted volume ratios, and since the supernatant phase is of larger volume, it is more similar to this.

Characterization of NaC10-Q680 2 wt% Tris water dilution series

This NaC10-Q680 2 wt% water dilution series including Tris, differs from the previous series due to the constant (S/P) ratio. This is because the surfactant and polymer are diluted. The visual appearance of the series is presented in Figure 4.26 followed by the pH and (S/P) values in Table 4.6. There is no difference in turbidity behaviour and viscosity when visually comparing the same series with the pH adjusted series without Tris. Furthermore, turbidity is observed for the samples with 1 and 2 wt% NaC10.

Figure 4.26: Visual appearance for 10, 5, 2, 1, 0.5, 0.2 and 0.1 wt% NaC10-0.1 wt%- Q680 2 wt% with Tris water dilution series.

Table 4.6: (S/P) and pH values (± pH 0.05) after three days for dilution series NaC10 2 wt% Q680 Tris, Water dilution.

NaC10 [wt%]	pH	(S/P)
10	9.22	9.58
5	9.13	
2	**8.93****	
1	**8.88****	
0.5	8.94	
0.2	8.97	
0.1	8.99	

The DLS results for NaC10- Q680 2 wt% including Tris, water dilution series is presented in Figure 4.27. For the higher concentration samples 5 and 10 wt% NaC10, signals at sizes 2-11 nm is present with two to three populations. Similarly to the polymer dilution of this series in the previous section, these signals correspond to the polymer and micelles.

The intermediate concentrations 1 and 2 wt% are turbid, and the signals are insignificant. This is except for a small peak for the 2 wt% samples at the size 5-6 nm, which could be explained by one of the alternatives for the previous higher concentrations. The lower concentrations, 0.2 and 0.5 wt%, have a small population which decreases with concentration, at the size 3-4 nm, corresponding to the polymer. For the sample 0.1 wt% almost no signal can be distinguished below 100 nm, which is reasonable because the system is highly diluted. All

signals around or above 100 nm for all samples are classified as contamination or artefacts. To conclude, the trend of the water dilution series is similar to the previous series, except that the polymer peak is not present at lower surfactant concentrations.

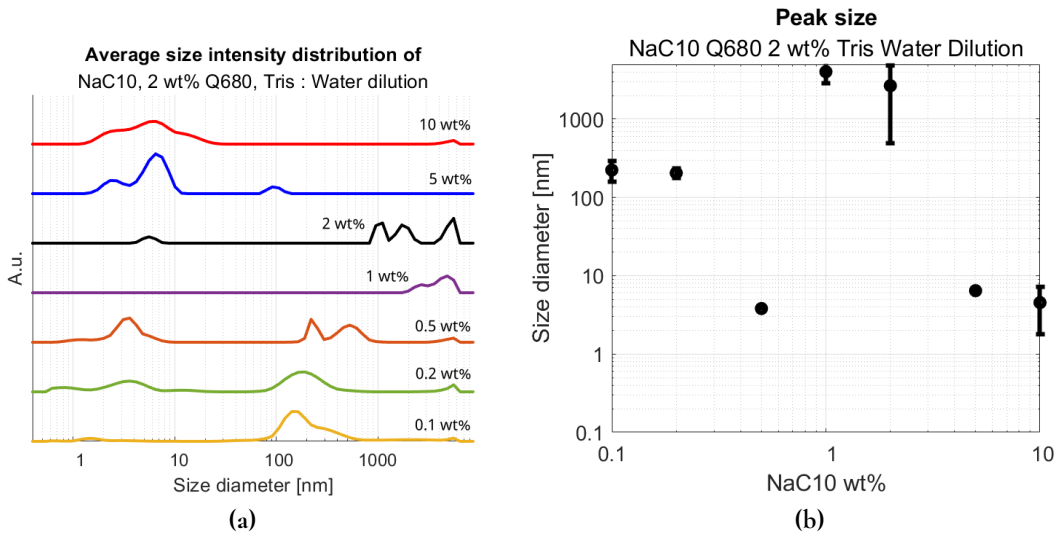

Figure 4.27: DLS results for NaC10 0.1-10 wt%- Q680 2 wt% including Tris water dilution series. (a) The average intensity size distribution results. (b) The average size of the largest population with error bars for standard deviation error of the averaging.

Ternary phase diagram of NaC10-Q680 Tris series

The sample matrix presented so far in this work for the NaC10-Q680 2wt% with the Tris system is translated into a partial ternary phase diagram as water is added as a dimension and is presented in Figure 4.28. The components of the system are NaC10, Q680, and water. The concentration of NaCl and Tris throughout the sample matrix is constant. Therefore they are not added as further dimensions but included in the water phase. Two different phases are present in the phase diagram. The areas in light grey represent a one-phase homogeneous behaviour. The area in dark grey represents a two-phase region where coacervation occurs. This two-phase region is delimited by the samples that were marked as turbid in the sample matrix, Figure 4.19. All samples with a NaC10 concentration of 1-2 wt% were in the coacervate formation region. Therefore, the coacervate formation is always observed around the surfactant's CMC and seems to be independent of the (S/P) = 1. Moreover, considering that there is a high salinity content in the system (> 0.5 wt% NaCl), the CMC is further decreased for the surfactant than according to literature (approximately 1.5 wt% for NaC10). This may further support the idea of coacervation occurring in a surfactant concentration at 1 to 2 wt%. Furthermore, apart from CMC, CAC is present and below CMC and helps with the formation of premicellar aggregates that allows coacervation to happen below CMC. In conclusion, this area of coacervation around CMC is the identified coacervate formation window for the system NaC10, Q680.

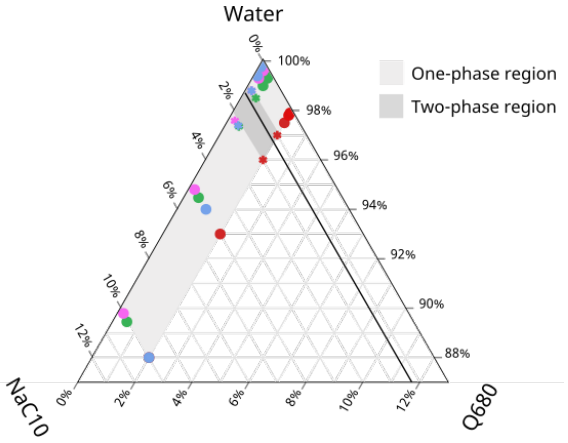

Figure 4.28: Ternary phase diagram of the surfactant-polymer-water system with NaC10 and Q680, including Tris. The axis consists of surfactant (0.1-10 % NaC10), polymer (0-2 % Q680) and water (98-100 %). The line is the approximate CMC for NaC10.

4.2.4 Mixed systems with cationic guar derivative

In this section, a different polymer-surfactant mixture was analyzed, where the QUATIN® polymer was exchanged for N-Hance. The polymers are both polysaccharides modified with positively charged groups. However, they are different in their chemical structure, seen in Figure 3.2 and Figure 3.3 in the Materials and Method section. The N-Hance has larger monomers and, therefore, lower charge densities in comparison to the QUATIN® polymers. The N-Hance polymer is firstly characterized, and then the surfactant-N-Hance system is studied.

Characterization of cationic guar derivative

NaC10-N-Hance samples with a concentration of 0.5 and 2 wt% N-Hance were prepared with the same background of Tris 20 mM and NaCl as all samples. It was prepared according to polymer dilution solution. The appearance of the 2 wt% N-Hance sample was slightly turbid and highly viscous, homogeneous. Meanwhile, the 0.5 wt% N-Hance was more water-like, minor turbid and exhibited phase separation with a little denser phase in the bottom of the vial.

The 2 wt% N-Hance sample was too viscous for DLS measurement since the gel phase has no diffusion or low diffusion. Therefore the DLS measurement was done on a lower concentration, 0.5 wt% N-Hance. The DLS result for the 0.5 wt% N-Hance sample is presented in Figure 4.29. The sample had signals at sizes above 10 nm, two peaks that overlap, one between 10-20 nm and one at 50 nm. Two other signals are observed at 200 and 450 nm. These peaks indicate aggregations of the polymer, compatible with the R_h of the polymer being 10-50 nm. Signals above 1000 nm are regarded as artefacts. Compared to the QUATIN® polymers, the N-Hance polymers are approximately ≥ 10 times larger. Nevertheless, the system was a bit turbid, with slight phase separation when letting rest. Therefore the DLS results cannot be regarded as entirely significant.

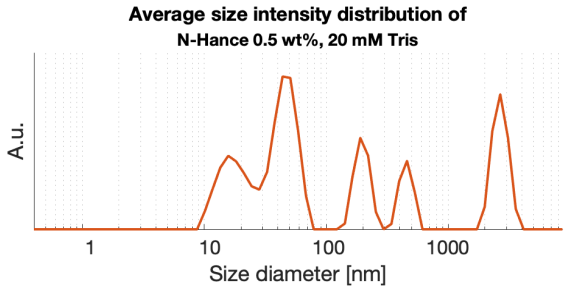

Figure 4.29: DLS results, particle size distribution, for sample 0.5 wt% N-Hance with 20 mM Tris.

The collected SAXS patterns for N-hance and Q680 at a concentration of 2 wt% are presented in Figure 4.30. For Q680, a plateau was observed for q-values below 0.1 $Å^{-1}$. N-hance instead exhibits a linear decay with a constant slope throughout the studied q-range. The different signal features for two polymers can be explained by their difference in molecular weight. Since the N-hance is a larger molecule, it has a higher intensity at lower q-values corresponding to larger distances and has not reached its plateau within this q-range.

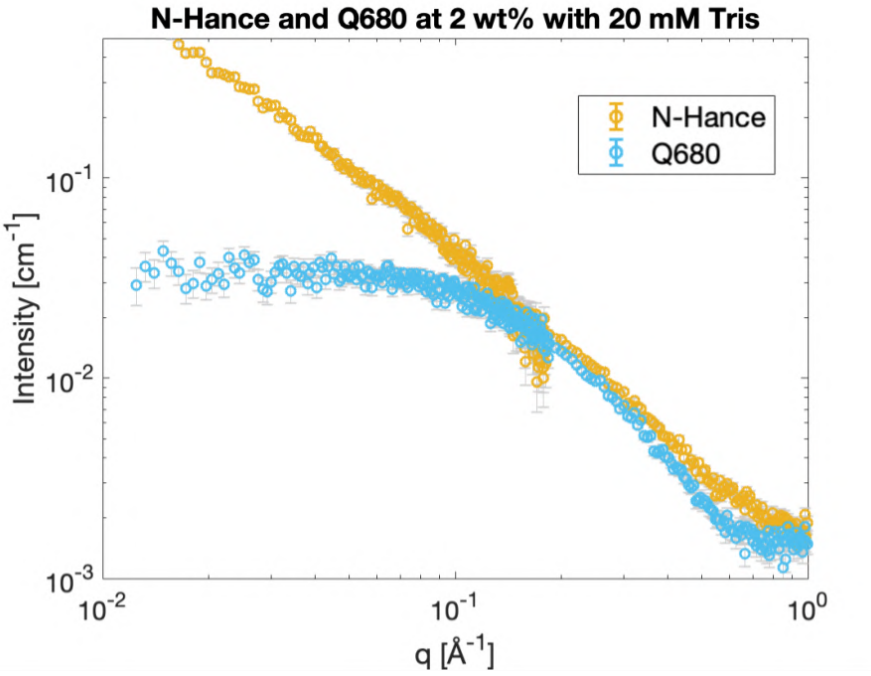

Figure 4.30: SAXS pattern for N-Hance and Q680 at a concentration of 2 wt% with 20 mM Tris.

The SAXS pattern of N-Hance with a concentration of 2 wt% was fitted with the Debye function, see Equation 3.1 in the method section. The fitting was performed to determine the polymer chains' R_g. This fitting is presented in Figure 4.11, and the R_g obtained with this fir is 97 Å. However, this should be considered a lower limit for the R_g since the q-range is too small for the signal, and the presence of a plateau at low q-values is essential for an accurate estimation of the R_g. Moreover, another possible interpretation is that the polymer chains could interconnect with each other in a tightly packed configuration, not allowing

for an approximation of the R_g of a single polymer chain. Nonetheless, the behaviour of the N-hance is considerably different from the Q680, where the approximated R_g to 9 Å, which is much smaller. This is compatible with that Q680 has a low degree of polymerisation and is below 60 units per polymer chain.

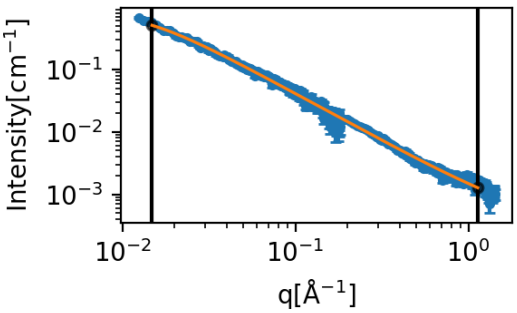

Figure 4.31: SAXS pattern for N-Hance 2w% together with the theoretical profile for the Gaussian chain, calculated with the the Debye function in SasView. The Radius of gyration was determined to 97 Å.

Characterization of NaC10-N-Hance dilution series.

A dilution series of 0.1-10 wt% NaC10 in an N-Hance 2 wt% water solution with Tris 20 mM and NaCl 0.525% was prepared, similarly to what was described in the previous chapter for NaC10-Q680. The visual appearance of these samples is presented in Figure 4.32. The dilution series are 10-0.1 wt% NaC10 and 2 wt% N-Hance. The 5 and 10 wt% NaC10 samples were macroscopically homogeneous, highly viscous and gel-like in texture immediately after preparation. Phase separation occurred for the other samples, 0.1-2 wt% NaC10. The top phase was almost clear and water-like in viscosity. Meanwhile, the bottom part was turbid and highly viscous, gel-like, and remained on the bottom of the vial when turned upside down. This more viscous phase indicates a higher concentration of colloidal agents, i.e. polymer and surfactant. An image of the 0.1 wt% NaC10 sample, where the phase separation is observed, is presented in Figure 4.32. As the samples were shaken, they became more homogeneous and turbid, indicating a microphase separation. However, they quickly phase separated again after a few seconds at rest. This phase separation was more pronounced for lower concentrations, 0.1-1 wt% NaC10, and still to some degree present for 2 wt% NaC10. Therefore, a critical limit in this behaviour is observed somewhere between these concentrations.

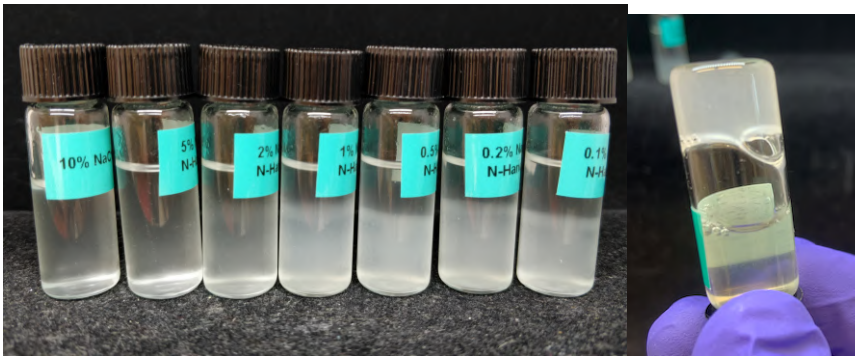

(a) (b)

Figure 4.32: The visual appearance of NaC10- N-Hance 2 wt% samples after preparation. (a) From left to right, the series 10, 5, 2, 1, 0.5, 0.2 and 0.1 wt% NaC10, after mixing and resting for 2 minutes. (b) Phase separation for sample 0.1 wt% NaC10- N-Hance 2 wt%. The sample is turned upside down and has a clear separation.

These N-Hance 2 wt% series had similar charge ratio (S/P) values as for the QUATIN series and therefore thought to be comparable, with (S/P) close to 1 for concentrations 0.5 and 1 wt% NaC10 N-Hance 2 wt%, see Table 4.7. Moreover, the pH for the N-Hance-series was between pH 9-10, higher than the QUATIN-series. According to its certificate of analysis, a system of 1 wt% N-hance in water has a pH of 10.7. The pH effect is more pronounced as the series decrease in NaC10 concentration.

Table 4.7: pH (± pH 0.05) and (S/P) values for 0.1-10 wt% NaC10, N-Hance 2 and 0.5 wt% series. All of the samples exhibited turbidity.

	N-Hance 2 wt%		N-Hance 0.5 wt%	
NaC10 [wt%]	pH	(S/P)	pH	(S/P)
10	9.3	23.68	9.24	94.72
5	9.5	11.50	9.27	46.96
2	9.67	4.60	9.11	18.78
1	9.92	2.30	9.05	9.39
0.5	10.27	1.15	9.14	4.70
0.2	10.52	0.46	9.19	1.88
0.1	10.37	0.23	9.24	0.94

The visual appearance of the NaC10- N-Hance 0.5 wt% is presented in Figure 4.33. All samples of this series were turbid after sample preparation. After three days of rest, phase separation occurred in the form of a small accumulation in the bottom of the vial. The phase separation happened to a lesser extent than in the previous 2 wt% N-Hance series.

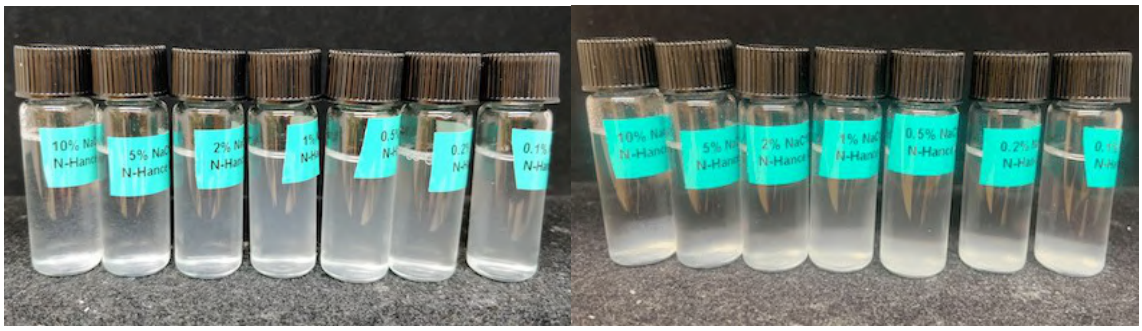

(a) (b)

Figure 4.33: Visual appearance of NaC10 10-0.1 wt%- N-Hance 0.5 wt%, series with Tris. (a) Just after preparation. (b) After resting for three days.

The SAXS pattern for the NaC10, N-Hance 2 wt% system for the concentration 2-10 wt% NaC10 is shown in Figure 4.34. The 1 and 2 wt% are from samples that exhibited a phase separation, both of these phases were studied with SAXS. The 1 and 2 wt% curves in Figure 4.34 correspond to the gel phase. All curves have features corresponding to the polymer being the linear slope at low q-values to 0.1 $Å^{-1}$. The 5 and 10 wt% curves have a distinct Gaussian peak with a peak maximum at $q \approx 18$ $Å^{-1}$, which corresponds to 35 Å. This peak is also present in the gel phase of the NaC10 1 and 2 wt%, but with much less intensity. The peak originates from the micellar structure of the surfactant aggregates.

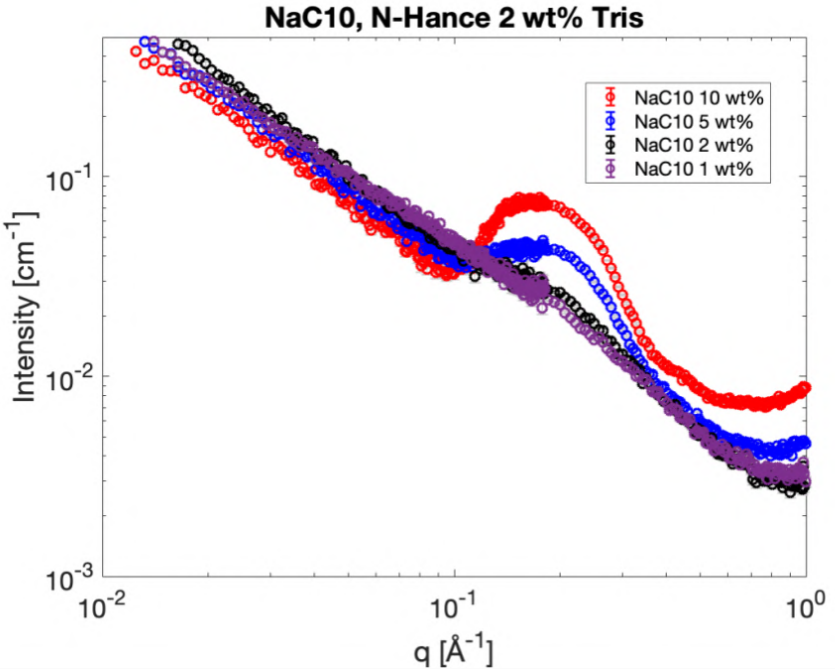

Figure 4.34: SAXS patterns for 2-10 wt% NaC10-N-Hance 2 wt% with 20 mM Tris.

SAXS measurements were also performed on the two phases for the 1 and 2 wt% samples that exhibited a phase separation to characterize these further. The collected SAXS patterns are presented in Figure 4.35. All of the curves exhibit features related to the polymer at low q-values. For the 2 wt% curves, there is a minor peak present at the region of the surfactant peak, with lower intensity. Suggesting that micelles are present in both phases in the samples, but some interactions make the signal less distinguishable. The intensity for the gel phase is higher throughout the entire studied q-range for both concentrations studied, indicating that both materials have accumulated in the gel phase. Interestingly, it is possible to observe features from both surfactant and polymer in both phases, suggesting that there is no strong enrichment of one of the components in one of the phases but rather a difference in concentrations. This is suggesting that coacervation happens in the samples that exhibit phase separation. A similar result was obtained for the 2 wt% NaC10- Q680 2 wt% sample, see Figure 4.25. However, for the Q680 sample, the difference in intensity between the two phases was much larger. Additionally, the gel phase was minimal for the Quatin samples. Meanwhile, the gel phase volume was approximately half of the samples' total volume for the N-Hance samples.

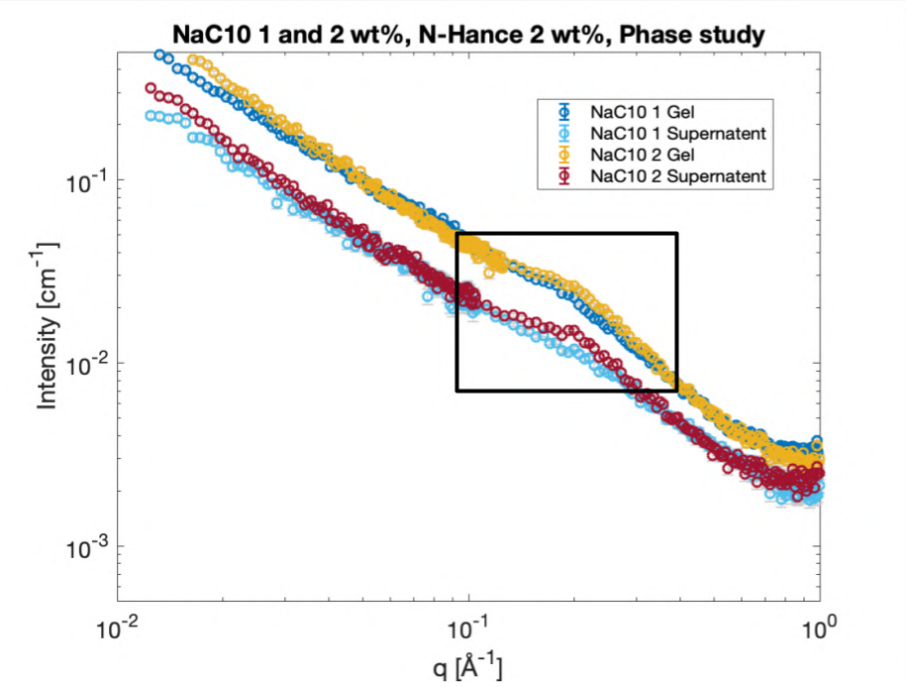

Figure 4.35: SAXS patterns for the gel and supernatent phase for the samples 1 and 2 wt% NaC10-N-Hance 2 wt% Tris. The black box shows the area where the surfactant peak is present.

4.3 Chapter 3 | Surface studies and deposition

4.3.1 Rinsing experiment, in-situ ellipsometry

Ellipsometry experiments were performed on NaC10-Q680 2 wt% system to characterize its deposition. The surface deposition was studied on a hydrophilic silica wafer for the ellipsometry experiments. The sample that was diluted during the rinsing experiment was a 10 wt% NaC10-Q680 2 wt% with Tris 20 mM. The water dilution solution contained: water, NaCl 0.525 wt% and Tris 20 mM, and in the polymer dilution solution, Q680 2 wt% was additionally added to the solution. In Figures 4.36 and 4.37, the thickness profile and mass deposition are respectively presented for the rinsing experiments. Moreover, in both figures, the rinsing start at 0 s. The signals before the experiment begins correspond to the 10 wt% NaC10 mixture, and at 1500 seconds, the diluting agent for the polymer dilution is changed to the water diluent.

In the rinsing experiment before 0 s, it can be seen that the 10 wt% NaC10 solution has been deposited with a layer thickness of 300 nm and with a mass of 0.5 mg/m^2. The signal is lost when the dilutiont runs for a few seconds because the sample becomes turbid. Since ellipsometry is an optical method, it cannot measure turbid samples due to all the scattering. The sample becomes turbid when it reaches the coacervate formation region. The signal returns after 200 seconds for both experiments, showing different behaviour. In the water dilution experiment, the signal for the deposited mass decreases in once the turbidity is reduced and the signal comes back, and it reaches a plateau value of 1.6 mg/m^2. Suggesting that more coacervates or other components deposit on the hydrophilic silica surface when the sample is turbid and unmeasurable. The layer thickness seems to increase after the turbid region, indicating that the layer formed in the turbid area has a higher density. The layer's mass and thickness seem to reach a plateau at 1.6 mg/m^2 and 90 Å, respectively, for low NaC10 concentrations. Implying that there is a deposition and some interaction between the deposited layer and the hydrophilic surface. It is energetically more favourable for the complexes formed on the surface to remain than desorb.

For the polymer dilution, the adsorbed amount increased after the turbid area before reaching its plateau value, in contrast to the water dilution, where it decreased. Implying that less was deposited in the turbid region when the polymer concentration was constant and not diluted. Moreover, at lower NaC10 concentrations, the adsorbed amount is around 2 mg/m^2. Finally, there seems to be a rather considerable variation in the thickness of the deposited layer. It is more reasonable that this is related to variation in data quality than the thickness. In conclusion, there is a deposition for both the water and polymer dilution experiments since the deposited mass is greater after the rinsing experiment. However, the amount deposited on the surface within the turbid region that includes the coacervation window is larger in the water dilution.

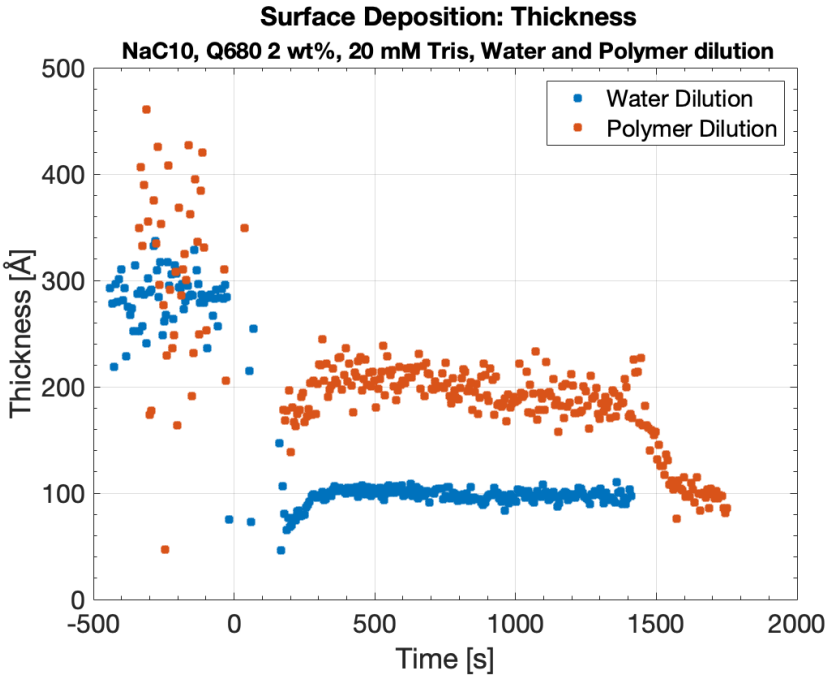

Figure 4.36: In-situ ellipsometry, thickness profile of for the water rinsing and polymer rinsing experiment of 10 wt% NaC10- Q680 2 wt%.

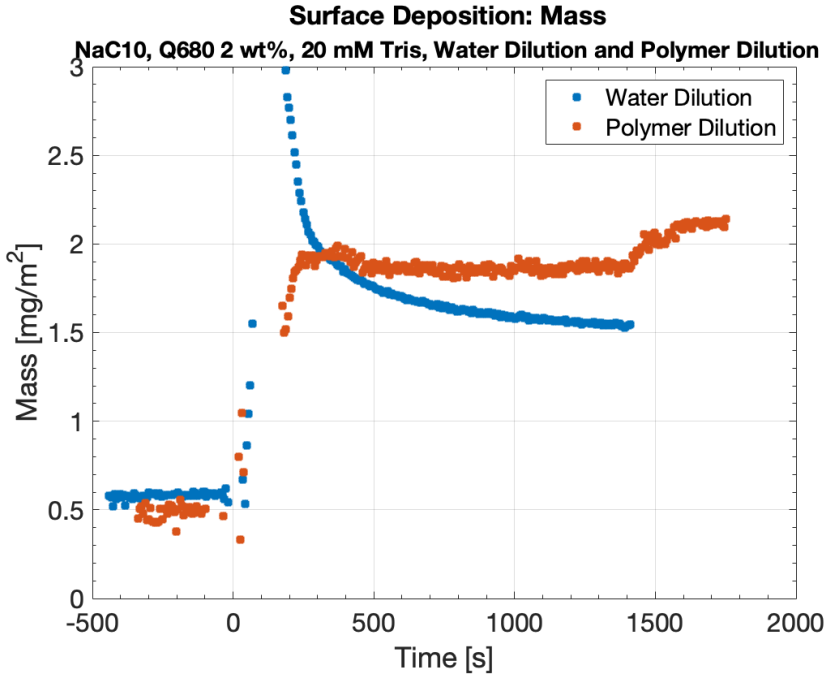

Figure 4.37: In-situ ellipsometry, mass profile for the polymer and water rinsing experiment of 10 wt% NaC10- Q680 2 wt%.

Chapter 5
Conclusion

In this study, different surfactant-polymer systems, with sodium and potassium caprate (NaC10, KC10) and sodium- and potassium laurate (NaC12, KC12) as surfactants, and the two cationic polymers QUATIN® and N-Hance have been studied. First as single ingredients and then in a wide concentration range, with visual inspection, DLS, SAXS and in-situ ellipsometry. Such systems were characterized in a wide composition range, where the surfactant concentration varied between 0.1 and 10% and the polymer from 0.02 to 2%.

Parameters investigated in this thesis are the following;

- **counter-ion** for the surfactant,
- **pH**, base vs buffer,
- **charge density** of polymer

Firstly the single ingredients were investigated. The solubility as a function of pH of the biobased surfactants C10 and C12 were evaluated with titration experiments with NaOH and KOH. The pKa was determined to be 7.6 for C10 and 8.6 for C12. Both C10 salts were observed to be soluble at room temperature, while NaC12 was not, and exhibited a Krafft temperature of 38 °C, and were therefore further investigated. From the titration curves, it was possible to infer that a pH above 9 was needed to have the surfactant in solution at room temperature. The CMC for NaC10 in water is reported in the literature as 1.5 wt%. For the conditions used in this work (NaCl 0.525%), this was expected to be slightly lowered. Such values are confirmed by DLS measurements that showed the presence of micelles (2-3 nm in size) for concentrations above 1 wt%.

The difference given by the different counter ions (sodium vs potassium) could be seen in the SAXS patterns collected for the different salts at 10 wt%, which is presented in Figure 4.7. The effect was seen on the surfactant feature at around 0.18 $Å^{-1}$, which is related to the difference in electron density between the core and shell of the micelles. The KC10 peak had a higher intensity, and its peak maximum was shifted to smaller q-values, .i.e larger sizes. This could be explained considering that Potassium is larger and heavier than Sodium. Therefore,

Potassium contributes to a larger size of the micelles for KC10, which is reflected in the shift of the surfactant feature to slightly lower q-values.

Three different cationic biopolymers were evaluated in this thesis. Two of them are Q350 and Q680, derivatives from inulin with higher charge densities, and the third is N-Hance, a Cat-Guar product. The N-Hance polymer has a higher molecular weight than the QUATIN® polymers. With a visual inspection, viscosity assessment, and more detail from DLS and SAXS, it is possible to conclude that the N-Hance forms aggregates with larger structures than quatin. Moreover, the largest population size for the QUATIN® polymers was 2-3 nm, and N-hance had populations with sizes above 10 nm.

The pH is a crucial parameter for the solubility of the surfactants, and their physical behaviour furthers the formation of micelles and coacervates. The pH for higher concentrations (10 wt% surfactant, 2 wt% QUATIN®) was around 9, which was adjusted by the base which formed the fatty acid salt. For lower concentrations, especially where the QUATIN® concentration was still high, the pH was observed to be decreased to 7. This was because the QUATIN® stock solution was at a lower pH (5). This lowering in pH shifts the equilibrium of the surfactant towards the acid form that is not soluble.

In order to prevent the pH shift and consequent surfactant precipitation, the pH was adjusted in all samples for the QUATIN® systems, both with dropwise addition of base and by the use of a buffer (Tris). To study the possible impact of Tris on the system, a new sample set was prepared in the presence of Tris and characterized as the previous. Such a study concluded that Tris had no effect on the system and successfully kept the pH around the desired value (9). Tris was also found more practical than the dropwise addition of base and therefore preferred.

The surfactant-polymer mixtures prepared were visually inspected in terms of viscosity and turbidity. The surfactant-QUATIN® were mostly water-like and clear. However, some samples exhibited turbidity; these were around the CMC of the surfactant. This suggests the presence of coacervate formation in a specific concentration window. The surfactant-N-Hance mixtures were viscous for higher polymer concentrations (2 wt%) and water-like for lower concentrations (2 wt%). Except 10 and 5 wt% surfactant, all samples exhibited phase separation for the N-Hance system. This phase separation also suggests coacervate formation.

The SAXS patterns for the mixed systems showed both the surfactant and polymer features; generally, no major signs of interactions were observed, except for samples 5wt% NaC10-Q680 2 wt% in both the water- and polymer dilution and 2wt% NaC10-Q680 2 wt% polymer dilution. For samples that exhibited a phase separation, SAXS patterns were collected for some samples to better understand both phases' composition.

A ternary phase diagram constructed for the NaC10-Q680 systems is presented in Figure 4.28. The mapped out coacervation region is within the concentration range 1-2 wt% of NaC10. The coacervation is observed for systems around the CMC of the surfactant. This includes slightly below the CMC, where premicellar aggregates might have facilitated coacervation, i.e., above CAC. This occurs regardless of polymer concentration. Hence, the (S/P) ratio does not have as significant an impact as initially thought. Thus, the CMC is a crucial parameter for the formation of coacervates for the surfactant-Q680 systems.

To better characterize the coacervate formation in terms of ability of depositing on surfaces, ellipsometry measurement were performed, where the 10% NaC10-Q680 2% system was diluted with both water and a Q680 2% water solution. The ellipsometry experiments showed that the adsorbed amount on the silica surface was larger for the water dilution than

the polymer dilution inside the coacervation window. Additionally, at high degrees of dilutions, i.e. low concentrations of surfactant, the deposited amount for the polymer dilution was 2 mg/mm^2 and 1.5 mg/mm^2 for the water dilution. The thickness of the adsorbed layers was 200 nm for the polymer- and 100 nm for the water dilution. In conclusion, the system is proven to deposit on a hydrophilic surface and function in the same way a shampoo formulation would.

The need for more environmentally friendly, biodegradable and sustainable products is a great driving force for development today. This thesis aimed to deepen the understanding of natural-based surfactants and polymers and their behaviour in bulk conditions and contact with surfaces to be more readily used for the development of greener formulations in various fields, such as personal care, pharmaceuticals or food.

References

[1] Sakamoto K, Lochhead R, Maibach H, Yamashita Y. Cosmetic science and technology: theoretical principles and applications. Elsevier; 2017.

[2] Peker S, Helvacı S, Yener B, İkizler B, Alp A. The Particulate Phase: A Voyage from the Molecule to the Granule. Solid-liquid two phase flow. 2008;p. 1–70.

[3] Akhlaghi N, Riahi S. Salinity effect on the surfactant critical micelle concentration through surface tension measurement. Iranian Journal of Oil and Gas Science and Technology. 2019;8(4):50–63.

[4] Baccile N, Seyrig C, Poirier A, Alonso-de Castro S, Roelants SL, Abel S. Self-assembly, interfacial properties, interactions with macromolecules and molecular modelling and simulation of microbial bio-based amphiphiles (biosurfactants). A tutorial review. Green Chemistry. 2021;23(11):3842–3944.

[5] Hayes DG. Fatty acids–based surfactants and their uses. Fatty acids. 2017;p. 355–384.

[6] Cistola DP, Hamilton JA, Jackson D, Small DM. Ionization and phase behavior of fatty acids in water: application of the Gibbs phase rule. Biochemistry. 1988;27(6):1881–1888.

[7] Small DM. Physical properties of fatty acids and their extracellular and intracellular distribution. In: Nestle nutrition workshop series (USA); 1992. .

[8] Cistola DP, Hamilton JA, Jackson D, Small DM. Ionization and phase behavior of fatty acids in water: application of the Gibbs phase rule. Biochemistry. 1988;27(6):1881–1888.

[9] Beare-Rogers J, Dieffenbacher A, Holm J. Lexicon of lipid nutrition (IUPAC Technical Report). Pure and applied chemistry. 2001;73(4):685–744.

[10] Niaounakis M. Biopolymers: processing and products. William Andrew; 2014.

[11] Niness KR. Inulin and oligofructose: what are they? The Journal of nutrition. 1999;129(7):1402S–1406S.

[12] QUATIN® [Internet]. Cosun; [cited 2022 05 15]. Available from: https://www.cosunbiobased.com/markets/personal-care/haircare/quatin/1.

[13] Uddameri V, Morse A, Tindle KJ. Hydraulic fracturing impacts and technologies: A multidisciplinary perspective. CRC Press; 2015.

[14] Keating CD. Liquid-liquid Phase Coexistence and Membraneless Organelles. Academic Press; 2021.

[15] Kakizawa Y, Miyake M. Creation of new functions by combination of surfactant and polymer-complex coacervation with oppositely charged polymer and surfactant for shampoo and body wash. Journal of oleo science. 2019;p. ess19081.

[16] Aramaki K, Shiozaki Y, Kosono S, Ikeda N. Coacervation in Cationic Polyelectrolyte Solutions with Anionic Amino Acid Surfactants. Journal of Oleo Science. 2020;p. ess20159.

[17] De Kruif CG, Weinbreck F, de Vries R. Complex coacervation of proteins and anionic polysaccharides. Current opinion in colloid & interface science. 2004;9(5):340–349.

[18] Timilsena YP, Akanbi TO, Khalid N, Adhikari B, Barrow CJ. Complex coacervation: Principles, mechanisms and applications in microencapsulation. International journal of biological macromolecules. 2019;121:1276–1286.

[19] Weinbreck F, Nieuwenhuijse H, Robijn GW, De Kruif CG. Complexation of whey proteins with carrageenan. Journal of Agricultural and Food Chemistry. 2004;52(11):3550–3555.

[20] Stanley F, Warner A, Schneiderman E, Stalcup A. Rapid determination of surfactant critical micelle concentrations using pressure-driven flow with capillary electrophoresis instrumentation. Journal of Chromatography A. 2009;1216(47):8431–8434.

[21] N-Hance™ CCG45 [Internet]. Ashland; [cited 2022 05 15]. Available from: https://www.chempoint.com/products/ashland/ashland-guar-and-guar-derivatives/n-hance-guar-and-conditioning-polymers/n-hance-ccg45.

[22] Schnablegger H, Singh Y. The SAXS guide: getting acquainted with the principles. Austria: Anton Paar GmbH. 2011;p. 1–124.

[23] Long MA, Kaler EW, Lee SP, Wignall GD. Characterization of lecithin-taurodeoxycholate mixed micelles using small-angle neutron scattering and static and dynamic light scattering. The Journal of Physical Chemistry. 1994;98(16):4402–4410.

[24] Manalastas-Cantos K, Konarev PV, Hajizadeh NR, Kikhney AG, Petoukhov MV, Molodenskiy DS, et al. ATSAS 3.0: expanded functionality and new tools for small-angle scattering data analysis. Journal of Applied Crystallography. 2021;54(1):343–355.

[25] SasView [homepage on the Internet]. SasView; 2022 [updated 2022; cited 2022 May 10]. Available from: https://www.sasview.org/about/.

[26] Polymer excluded volume [homepage on the Internet]. SasView; unknown [updated unknown; cited 2022 May 10]. Available from: https://www.sasview.org/docs/user/models/polymer_excl_volume.html.

[27] Core shell sphere [homepage on the Internet]. SasView; unknown [updated unknown; cited 2022 May 10]. Available from: https://www.sasview.org/docs/user/models/core_shell_sphere.html.

[28] Svensson AV, Johnson ES, Nylander T, Piculell L. Surface deposition and phase behavior of oppositely charged polyion- surfactant ion complexes. 2. A means to deliver silicone oil to hydrophilic surfaces. ACS Applied Materials & Interfaces. 2010;2(1):143–156.

[29] McBain JW, Sierichs WC. The solubility of sodium and potassium soaps and the phase diagrams of aqueous potassium soaps. Journal of the American Oil Chemists Society. 1948;25(6):221–225.

[30] Joshi J, Aswal V, Bahadur P, Goyal P. Role of counterion of the surfactant molecule on the micellar structure in aqueous solution. Current Science. 2002;p. 47–49.

Appendices

Appendix A

Visual appearance of mixed systems without adjustments of pH

Visual appearance Q350

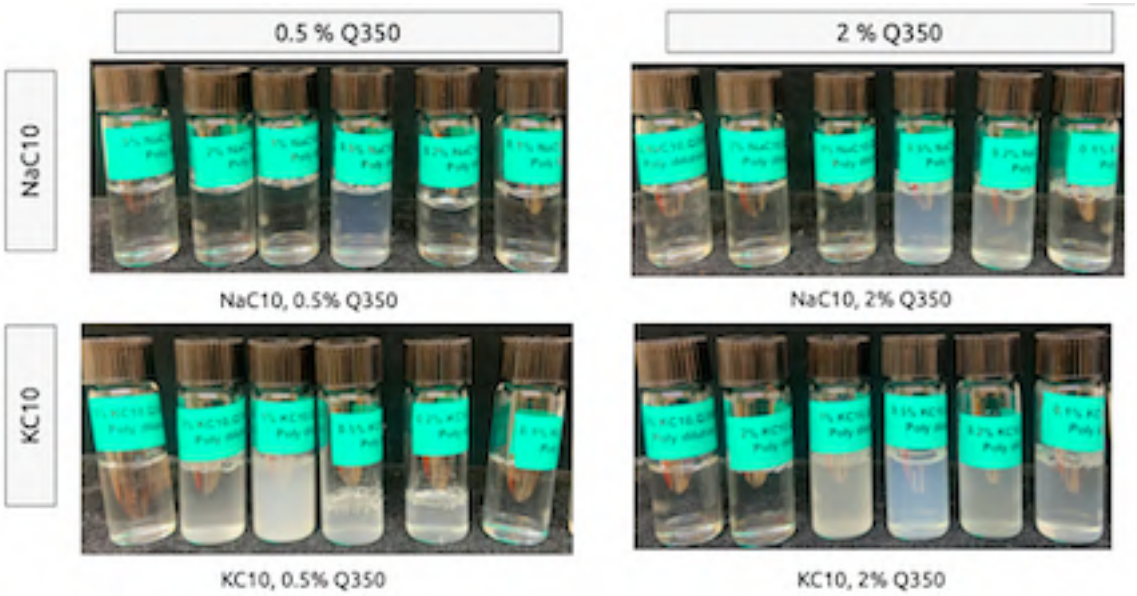

(a) Polymer dilutions

Figure A.1: Visual appearances of series of 5-0.1 wt% NaC10- Q350. polymer dilutions.

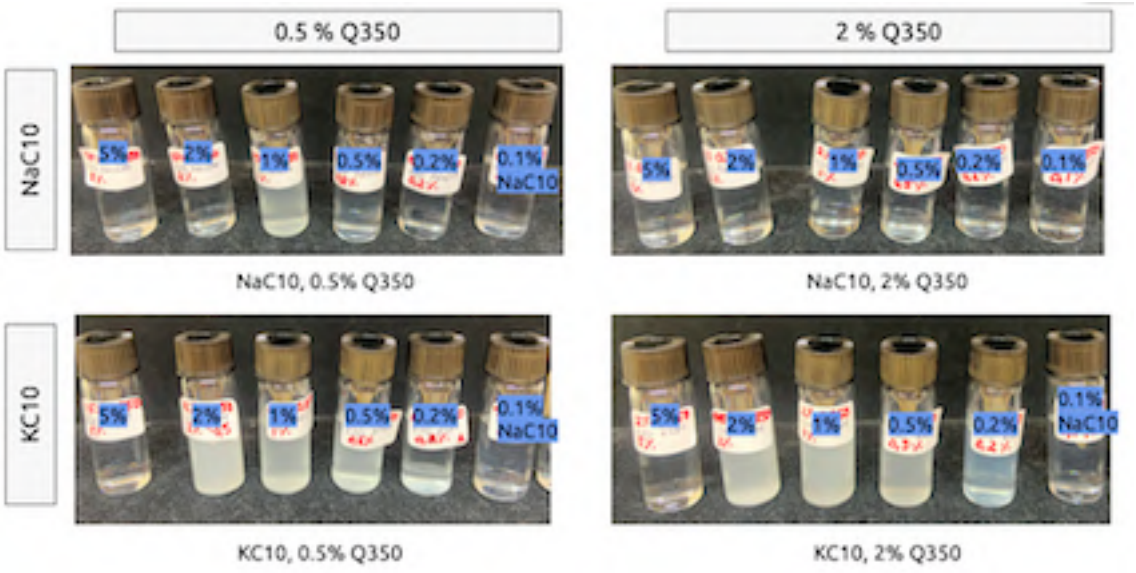

(a) Water dilutions

Figure A.2: Visual appearances of series of 5-0.1 wt% NaC10- Q350. water dilutions.

Visual Appearance Q680

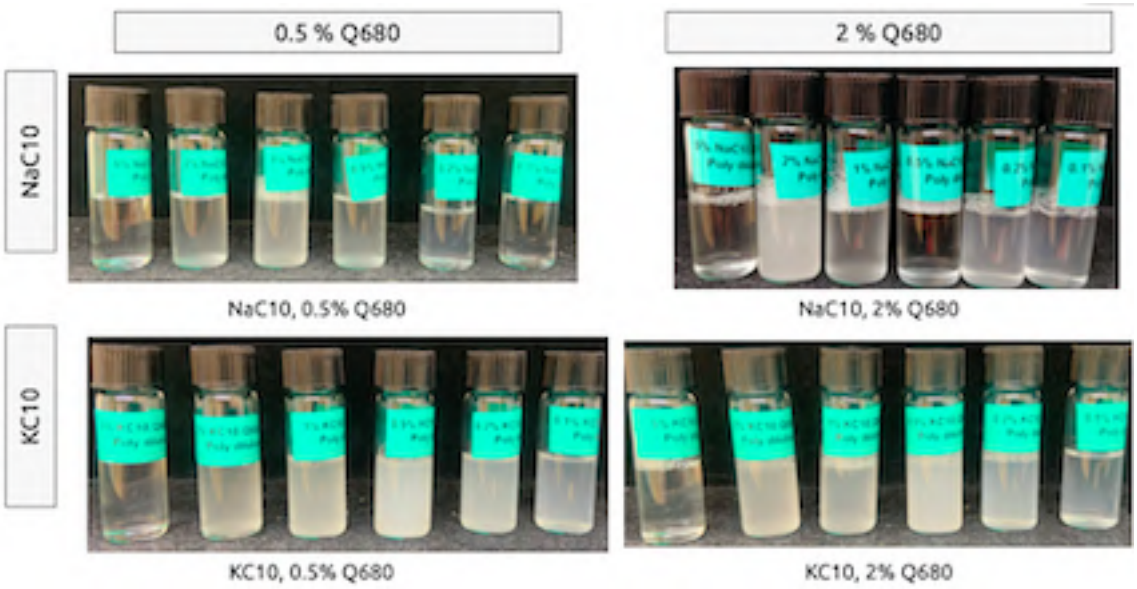

(a) Polymer dilutions

Figure A.3: Visual appearances of series of 5-0.1 wt% NaC10- Q680. polymer dilutions

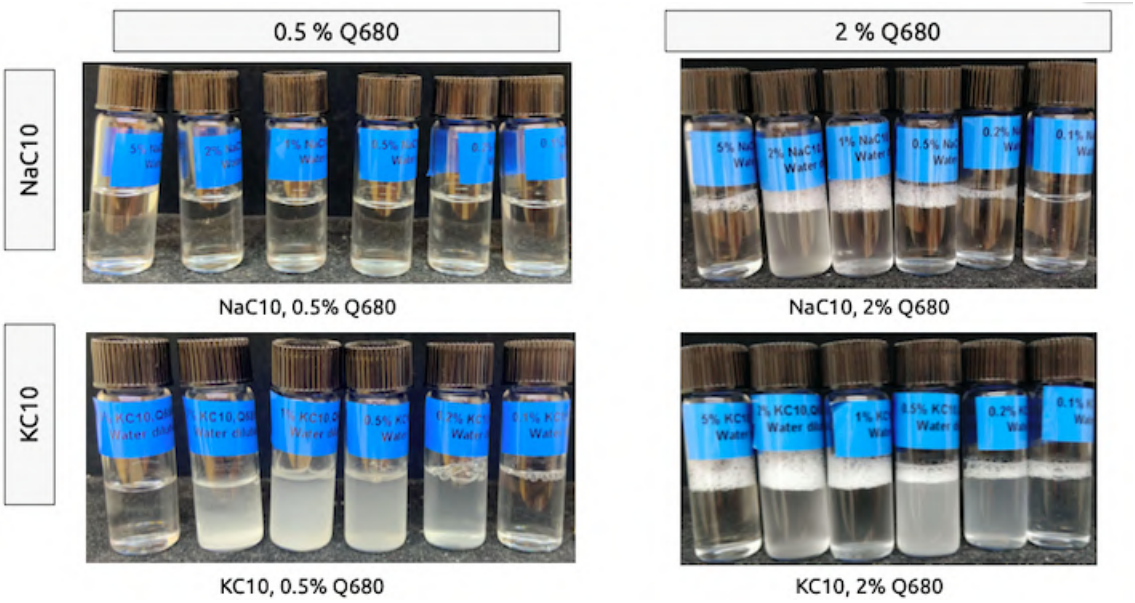

(a) Water dilutions

Figure A.4: Visual appearances of series of 5-0.1 wt% NaC10- Q680. water dilutions.

Appendix B

Visual appearance of mixed systems with adjustments of pH

NaC10-Q350

(a) Before pH adjustment **(b)** After pH adjustment

Figure B.1: Visual appearance of 5-0.1 wt% NaC10- Q350 2 wt % polymer dilution solution serie, before and after adjusted to pH 9.

Table B.1: pH values before and after adjustment and surfactant/poly(+) charge ratio for the NaC10-Q350 2 wt% water dilution solution series.

NaC10 [wt%]	(S/P)	pH Before	pH After
5	7.55	9.21	9.01
2	3.02	8.51	9.06
1	1.51	7.93	9.39
0.5	0.76	7.41	9.14
0.2	0.30	6.89	9.07
0.1	0.15	6.42	9.15

NaC10-Q680

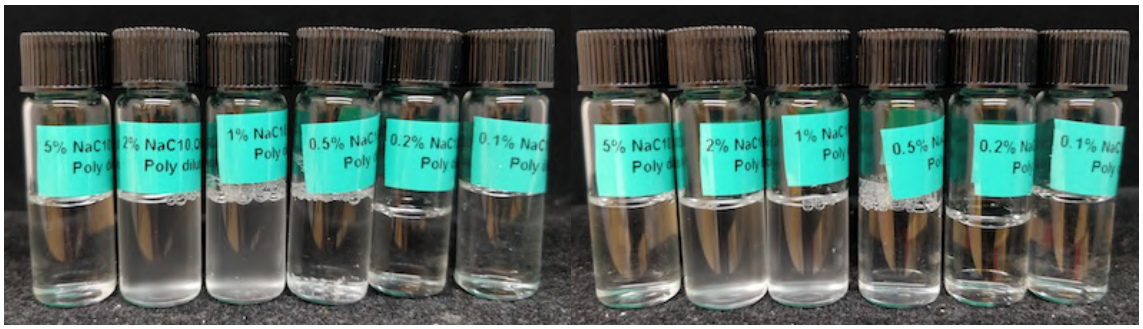

(a) Before pH adjustment (0.5 wt% Q680)

(b) After pH adjustment (0.5 wt% Q680)

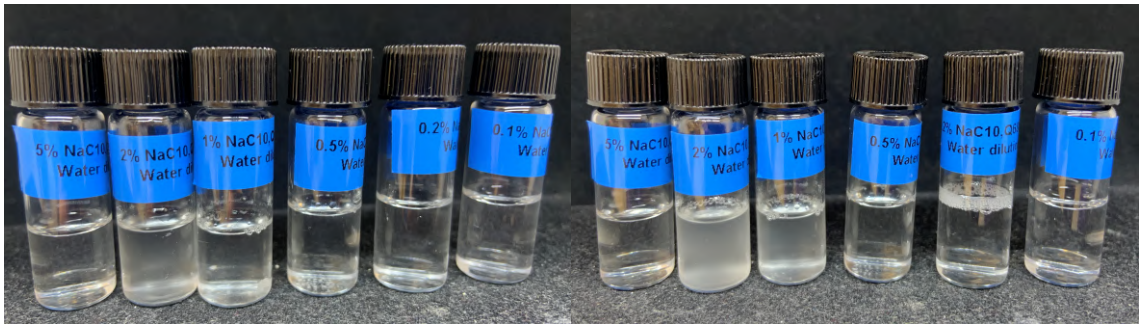

(c) Before pH adjustment (2 wt% Q680, water dilution)

(d) After pH adjustment(2 wt% Q680, water dilution)

Figure B.2: Visual appearance of 5-0.1 wt% NaC10-Q680 0.5 or 2 wt% polymer dilution solution series (green) and water dilution series (blue). Before and after adjusted to pH 9. The lower concentrations 0.1-0.5 wt% C10 lost turbidity after pH adjustment.

Table B.2: pH values before and after adjustment to pH 9and surfactant/poly(+) charge ratio for the NaC10-Q680 2 wt% polymer dilution solution series.

NaC10 [wt%]	(S/P)	pH Before	pH After
5	4.74	9.06	9.06
2	1.90	8.70	9.02
1	0.95	8.19	9.02
0.5	0.47	7.48	9.00
0.2	0.19	6.80	9,12
0.1	0.09	6.32	9.04

Table B.3: pH values before and after adjustment and surfactant/poly(+) charge ratio for the NaC10-Q680 2 wt% water dilution solution series.

NaC10 [wt%]	(S/P)	pH Before	pH After
5	9.48	9.16	9.07
2		8.73	9.06
1		8.15	8.96
0.5		7.98	9.42
0.2		8.03	8.98
0.1		8.23	9.53

KC10-Q680

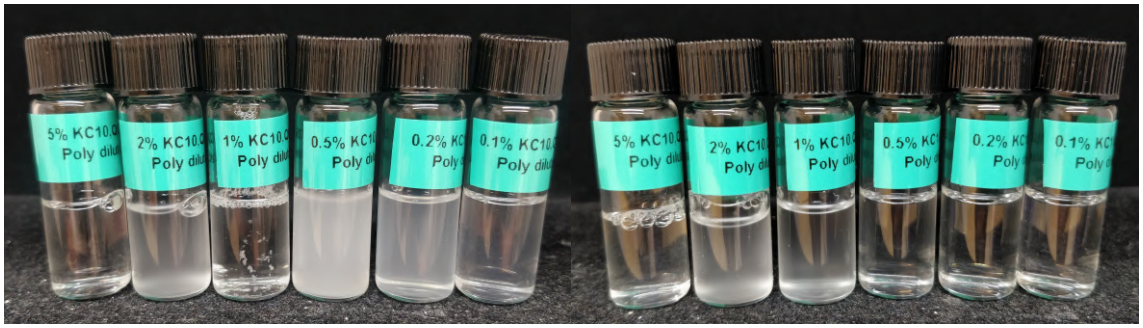

(a) Before pH adjustment **(b)** After pH adjustment

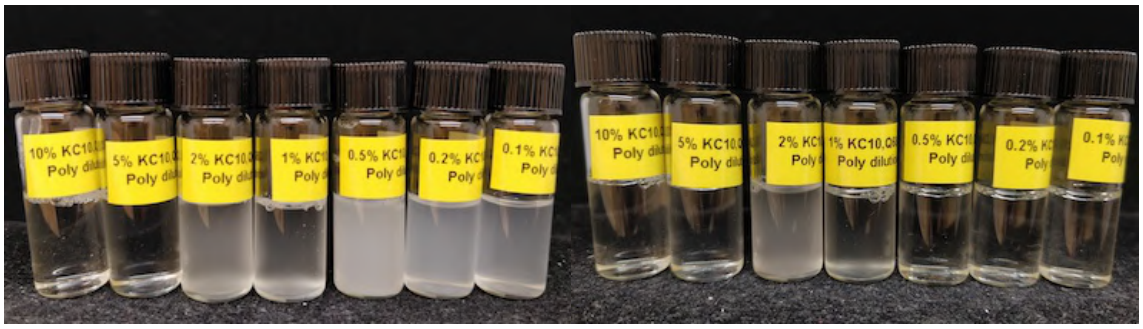

(c) Before pH adjustment **(d)** After pH adjustment

Figure B.3: Visual appearance of two series of 10/5-0.1 wt% KC10-Q680 2 wt% series, before and after adjustment to pH 9. The lower concentrations 0.1-0.5 wt% KC10 samples lost turbidity after pH adjustment.

Table B.4: Table summarizing the pH values before and after adjustment and surfactant/poly(+) charge ratio for the KC10, Q680 2 wt% polymer dilution.

KC10 [wt%]	(S/P)	pH Before	pH After
5	4.38	8.5	9.0
2	1.75	8.16	9.19
1	0.88	7.8	9.04
0.5	0.44	7.37	9.4
0.2	0.18	6.72	9.22
0.1	0.09	6.48	9.2

Appendix C

Visual appearance of mixed systems with Tris

NaC10-Q680 Tris

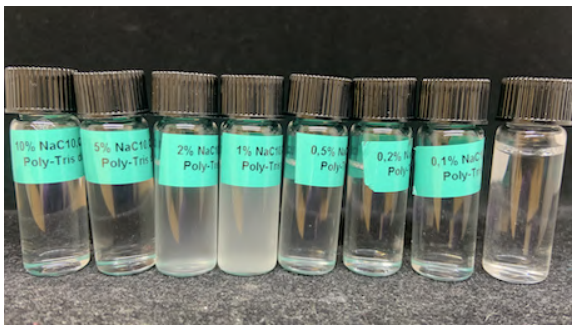

(a) After preparation

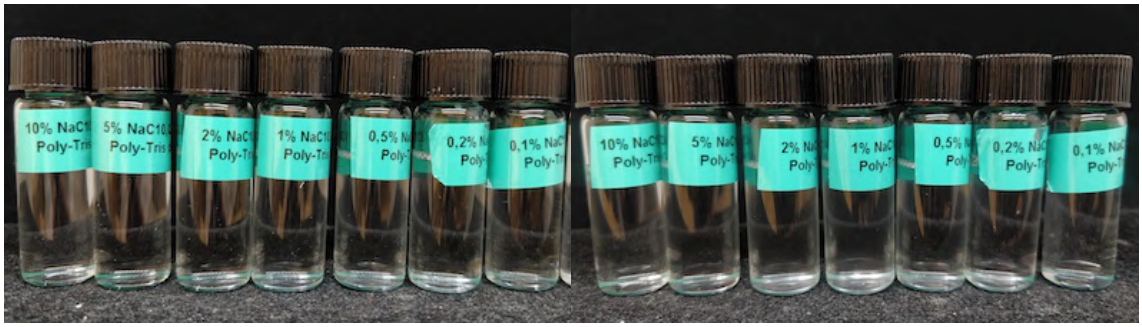

(b) 3 days rest **(c)** 3 days rest + shaking

Figure C.1: Visual appearance of 10-0.1 wt% NaC10- Q680 0.2 wt % including Tris, polymer dilution series.

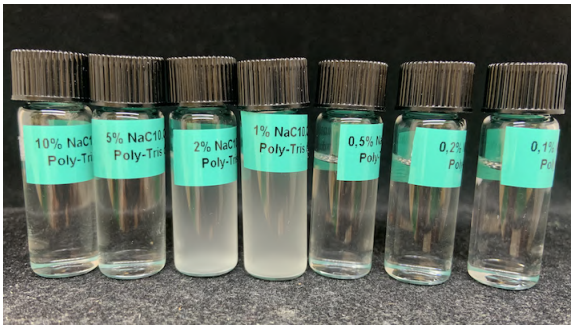

(a) After preparation (0.5)

(b) 3 days rest

(c) 3 days rest + shaking

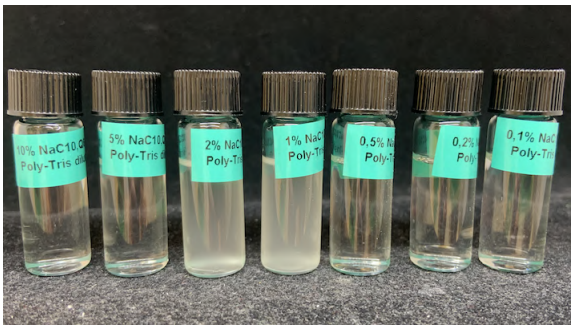

(d) After preparation (2 wt)

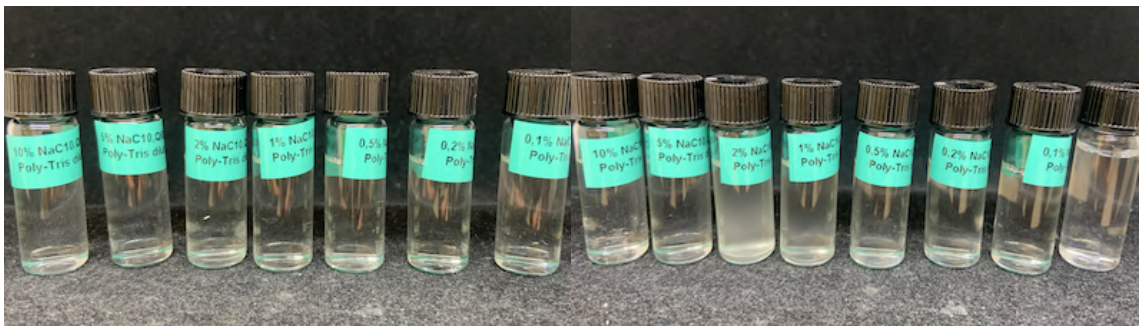

(e) 3 days rest (2 wt)

(f) 3 days rest + shaking

Figure C.2: Visual appearance of 10-0.1 wt% NaC10- Q680. (a, b, c) Q680 0.5 wt% and (d, e, f) Q680 2 wt % including Tris, polymer dilution series. Shaking method: oscillating instrument.

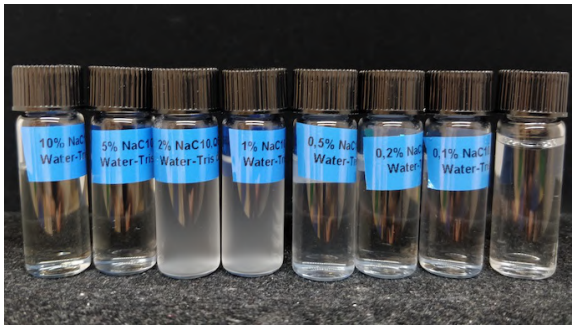

(a) After preparation

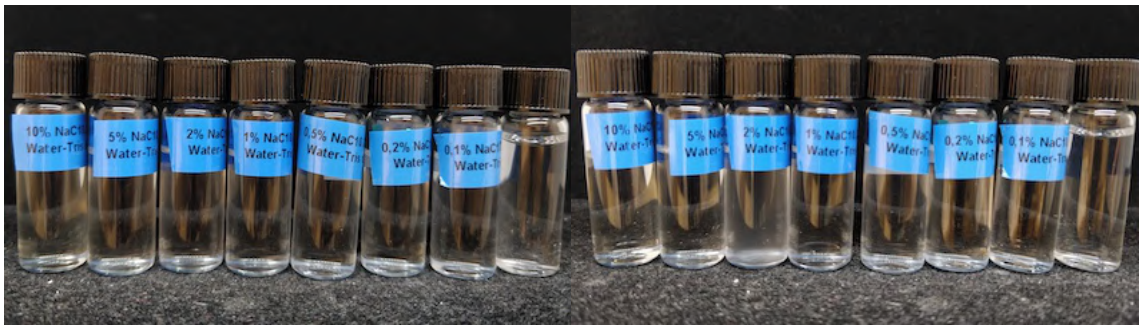

(b) 3 days rest

(c) 3 days rest + shaking

Figure C.3: Visual appearance of 10-0.1 wt% NaC10- Q680 2 wt % including Tris, water dilution series. Shaking method: oscillating instrument.

EXAMENSARBETE Green Coacervates for Pharma and Food
STUDENTER Izabella Imets, Andreas Vallin
HANDLEDARE Tommy Nylander (LTH), Marta Gubitosi (CR Competence AB)
EXAMINATOR Marie Wahlgren (LTH)

Biobaserade ingredienser för ersättning av fossilbaserade ingredienser inom läkemedels- och matbranschen på sikt

POPULÄRVETENSKAPLIG SAMMANFATTNING **Izabella Imets, Andreas Vallin**

Behovet av biobaserade ingredienser har ökat med den hållbara utvecklingen, och därmed har kraven på producenter ökat. En av dessa ingredienser kallas "koacervat", som används i många produkter idag, exempelvis i kosmetika, läkemedel och matvaror. Koacervat har unika egenskaper som utvärderats i detta examensarbete.

I dagens samhälle är de flesta produkter inom kosmetika-, läkemedels- och matbranschen baserade på fossilbaserade ingredienser som utvinns från råolja och med de nuvarande klimatproblemen forskas och undersöks det intensivt efter möjligheter till förnybara alternativ. I många produkter från dessa områden finns det ofta ett kemiskt komplex, mellan två större molekyler med olika laddningar. Dessa komplex, kallas “koacervat” och syftet med dem i många formuleringar är att fästa sig vid olika ytor och utföra olika uppdrag beronde på formuleringen.

Vidare är det främst koacervatingredienserna som utgör dessa komplex man vill ersätta. Vanligtvis, består komplexen av surfaktanter och polymer med olika laddningar. Mekanismerna som skapar dessa komplex är invecklade och många faktorer kan vara orsaken bakom. Däremot, är gängse teori att om man har lika mängder laddning av surfaktant och polymer i systemet är det optimalt för koacervat formation. I detta scenario har vi laddningsneutralitet. Koacervat måste vara i en vattenlösning för det ska skapas. När väl formationen sker resulterar det i en uppdelningen av två olika vätskor med olika densititer. Vätskan med högre densitet kallas koacervat och lägger sig på botten.

I detta examensarbete har vi undersökt särskilda biobaserade surfaktanter, som är mellanstora fettsyror (kaprinsyra och laurinsyra) utvunnen från kokosolja och palmkärnor. Biopolymererna som undersöktes är inulinbaserade utvunna från cikoriarötter. Dessa ingredienser kombinerades i olika surfaktantpolymerkombinationer där särskilda parametrar undersöktes. Karakteriseringen genomfördes med hjälp av två spridningstekniker av ljus- och röntgenvågor.

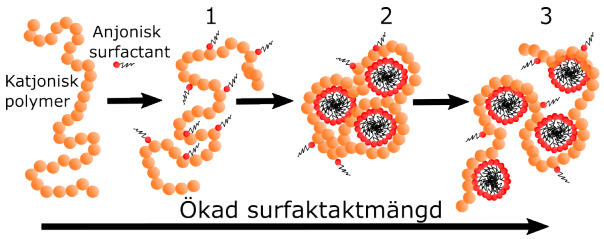

Beteendet mellan surfaktanter och polymerer i förhållande till ökad surfaktantkoncentration.

Resultatet av formation av koacervat gavs främst från parametrarna; pH-värde över 9, för lösligheten av surfaktanterna; en viss koncentration av surfaktanterna för att de skulle kunna bilda miceller, där surfaktanterna bildar egenordnade, runda strukturer. Resultaten visade också att koacervatformation kunde ske långt ifrån laddningsneutralitet.